The chromodomain proteins, Cbx1 and Cbx2 have distinct roles in the regulation of heterochromatin and virulence in the fungal wheat pathogen, *Zymoseptoria tritici.*

Running Title: *Z. tritici* chromodomain proteins, Cbx1 and Cbx2.

Callum J. Fraser[1], Julian C. Rutherford[1], Jason J. Rudd[2] and Simon K. Whitehall[1]

[1]Biosciences Institute, Faculty of Medical Sciences, Newcastle University
Newcastle upon Tyne NE2 4HH, United Kingdom

[2]Biointeractions and Crop Protection, Rothamsted Research, Harpenden, AL5 2JQ, United Kingdom

Correspondence:
Email: simon.whitehall@ncl.ac.uk
Tel +44(0)1912085989

SUMMARY

Heterochromatin is characterized by specific histone post-translational modifications such as the di- and tri-methylation of histone H3 on lysine 9 (H3K9me2/3), which direct the recruitment of 'reader' proteins to chromatin. In the fungal phytopathogen, *Zymoseptoria tritici,* deletion of the H3K9 methyltransferase gene *kmt1,* results in a global increase in the expression of transposable elements (TEs), genome instability and loss of virulence. Here we have identified two *Z. tritici* chromodomain proteins, Cbx1 and Cbx2, that recognise H3K9me modifications. Cbx1 is a Heterochromatin Protein 1 homolog that binds H3K9me2/3 *in vitro* and associates with heterochromatic loci *in vivo*. Transcriptomic analysis also indicates that Cbx1 and Kmt1 regulate overlapping sets of protein-encoding genes. However, unlike Δ*kmt1* mutants, Δ*cbx1* strains do not exhibit a global increase in TE expression and have only a partial reduction in virulence, suggesting the existence of additional H3K9me reader proteins. Accordingly, we have identified a fungal-specific chromodomain protein, Cbx2, that binds H3K9me3 *in vitro*. Strikingly, the growth defects of Δ*cbx1* Δ*cbx2* double mutants closely resemble those of Δ*kmt1* consistent with Cbx1 and Cbx2 playing redundant roles in gene silencing. Overall, the data suggest that key functions of H3K9me modifications are mediated by a combination of Cbx1 and Cbx2.

KEY WORDS

Zymoseptoria tritici, heterochromatin, H3 lysine 9 methylation, chromodomain, heterochromatin protein 1 (HP1).

INTRODUCTION

Zymoseptoria tritici is a fungal pathogen of wheat that is responsible for septoria tritici blotch disease. The initial phase of infection (10-14 days) is characterised by symptomless intercellular colonisation of the stomatal cavity and evasion from detection through the secretion of chitin binding proteins and likely, factors that repress and manipulate the wheat immune response (Goodwin *et al.*, 2011, Lee *et al.*, 2014, Marshall *et al.*, 2011, Rudd, 2015, Steinberg, 2015, Canzio *et al.*, 2014, Kumar & Kono, 2020). The second stage of infection is marked by death of the plant cells lining the stomatal cavity and a switch to a necrotrophic growth phase (Rudd, 2015, Steinberg, 2015). The increase in nutrient availability allows a rapid increase in growth followed by the formation of pycnidia, the asexual fruiting bodies of *Z. tritici*, which appear as melanised black dots on the leaf surface (Steinberg, 2015). Unsurprisingly, the switch in lifestyle during the infection process is accompanied by a major reprogramming of the transcriptome (Kellner *et al.*, 2014, Rudd *et al.*, 2015), but the mechanisms by which this is achieved are poorly understood.

The colonization of plant tissue by fungal pathogens requires the expression of specific effector genes (Uhse & Djamei, 2018). Effector genes are often lowly expressed in axenic culture but are strongly upregulated during the infection process. In a number of plant-associated fungi, putative effector genes are located in heterochromatic regions of the genome that are often enriched with transposable elements (TEs) and subject to transcriptional silencing (Soyer *et al.*, 2015). Accordingly, the disruption of heterochromatin in the oil seed rape pathogen *Leptosphaeria maculuns* results in the de-repression of effector genes located in repeat rich regions (Soyer *et al.*, 2014) and the expression of genes that allow *Epichloe festucae* to form a mutualistic interaction with the grass species, *Lolium perenne* are

66 also regulated by heterochromatin (Chujo & Scott, 2014). These findings have led to
67 a model whereby reprogramming of heterochromatic regions of the genome regulates
68 effector gene expression programmes and facilitates plant colonization (Soyer *et al.*,
69 2015).

70 Heterochromatin is characterised by specific histone post translation
71 modifications (PTMs), notably di- and tri-methylation of histone H3 on lysine 9
72 (H3K9me2/3) and the tri-methylation of lysine 27 (H3K27me/3) (Allshire & Madhani,
73 2018). H3K9me2/3 is considered to be a hallmark of constitutive heterochromatin
74 whereas H3K27me3 in metazoans is commonly associated with facultative
75 heterochromatin that is reversible in response to appropriate stimuli (Allshire &
76 Madhani, 2018). Genome-wide mapping of these modifications in *Z. tritici* has revealed
77 that H3K9me2 is predominantly associated with TEs (Schotanus *et al.*, 2015).
78 H3K27me3 is associated with TEs but is also enriched at telomeres and on the
79 conditionally dispensable accessory chromosomes (Schotanus *et al.*, 2015). Deletion
80 of the H3K27 methyltransferase gene, *kmt6* results in increased expression of genes
81 located on accessory chromosomes but has only a subtle impact on virulence in wheat
82 infection assays (Möller *et al.*, 2019). In contrast, deletion of *kmt1*, which encodes the
83 H3K9 methyltransferase, results in growth defects *in vitro* and severely compromises
84 virulence (Möller *et al.*, 2019). H3K9me2/3 also plays a key role in maintaining
85 genome stability. In Δ*kmt1* strains, loci that were previously occupied by H3K9me3
86 are invaded by H3K27me3 which is accompanied by an increased frequency of large
87 scale chromosomal rearrangements and accessory chromosome loss (Möller *et al.*,
88 2019).

89 Histone PTMs modulate chromatin function by directing the recruitment of non-
90 histone proteins 'reader' proteins. Recognition of H3K9me2/3 is commonly achieved

by members of the Heterochromatin Protein 1 (HP1) family that have a conserved domain organisation comprised of an N-terminal chromodomain (CD), and a C-terminal chromoshadow domain (CSD) separated by a flexible hinge region (Canzio *et al.*, 2014, Kumar & Kono, 2020). The CD is responsible for the recognition of H3K9me2/3 whereas the CSD mediates homodimerization and provides a hub for the docking of interacting proteins (Bannister *et al.*, 2001, Cowieson *et al.*, 2000, Smothers & Henikoff, 2000). An HP1 dimer is capable of bridging two nucleosomes (Machida *et al.*, 2018) and it is proposed that CD-CD interactions drive the formation of oligomeric structures which condense chromatin and provide a platform for the assembly of additional heterochromatin components (Canzio *et al.*, 2014, Kumar & Kono, 2020).

Here we have identified and characterised the *Z. tritici* HP1 homolog, Cbx1. We find that Cbx1 and the H3K9 methyltransferase, Kmt1 regulate the expression of highly similar sets of protein encoding genes and that Cbx1 is enriched at H3K9me-marked loci. However, the removal of Cbx1 does not result in the phenotypes that are associated with loss of Kmt1, suggesting that *Z. tritici* has additional H3K9me-effectors. Consistent with this hypothesis, we show that a fungal-specific CD protein, Cbx2, binds to H3K9me3 *in vitro* and plays a role in the silencing of some Kmt1-regulated genes. Furthermore, genetic analysis is consistent with a model whereby key biological effects of H3K9me PTMs in *Z. tritici* are mediated by a combination of Cbx1 and Cbx2.

RESULTS

Cbx1 is a *Z. tritici* HP1 homolog that binds H3K9me2/3

Methylation of histone H3 on lysine 9 is required for the genome stability and virulence of *Z. tritici* (Möller *et al.*, 2019). Therefore, we sought to identify the 'reader' proteins that recognise this histone modification. In many organisms, H3K9me2/3 marks are bound by members of the HP1 family of Chromobox (Cbx) proteins. BLAST analyses of the *Z. tritici* genome sequence revealed a hypothetical protein ZtRRes_04004, (hereafter called Cbx1) with an N-terminal chromodomain (CD) and a C-terminal chromoshadow domain (CSD) that share high similarity with HP1 proteins from other fungi (Fig 1). The Cbx1 CD is flanked by an acidic N-terminal patch and basic C-terminal hinge region which are also characteristics of HP1-type proteins (Hiragami-Hamada & Nakayama, 2019).

While HP1 proteins typically exhibit specificity for H3K9me2/3, both *Tetrahymena* Hhp1 and *Arabidopsis* TFL2/LHP1 recognise H3K27me3 (Turck *et al.*, 2007, Yale *et al.*, 2016). This prompted us to assess the binding specificity of Cbx1. Full-length Cbx1 was expressed as a GST fusion protein in *E. coli* and purified by affinity and size exclusion chromatography. The binding capacity of GST-Cbx1 was then investigated using a pull-down assay with biotinylated histone H3 peptides. In these assays GST-Cbx1 exhibited a clear preference for H3K9me2 and H3K9me3 modified peptides. No preference for the H3K27me3 or H3K4me3 peptides relative to the unmodified H3 peptide control was observed (Fig 2A & B). These results indicate that Cbx1 is an HP1 family member that binds to H3K9me2/3 modifications *in vitro*.

The subcellular localisation of Cbx1 was determined by constructing a strain expressing a GFP-tagged fusion protein (*cbx1-GFP*) under the control of its own promoter. Fluorescence microscopy of *cbx1-GFP* cells revealed a strong nuclear GFP

signal (Fig 2C). Next, chromatin immunoprecipitation (ChIP) assays were used to investigate the ability of Cbx1 to associate with H3K9me-enriched regions of the genome (Fig 2D). A strong enrichment of Cbx1-GFP was observed at a TE (DTH_element 299 5_ZTIPO323) that is known to be associated with H3K9me (Schotanus *et al.*, 2015). Furthermore, a similar enrichment of Cbx1-GFP was also found at a H3K9me-marked subtelomeric region (Chromosome 1: 161011-175642). Importantly, Cbx1-GFP enrichment was not detected at the euchromatic (H3K4me3-associated) genes, *actin* (*Mycgr3G105948*) and *GAPDH* (*Mycgr3G99044*). Notably, *GAPDH*, is located adjacent to an H3K9me-marked DNA transposon, suggesting that the resolution of the assay was sufficient to distinguish between neighbouring H3K9me-marked and non-marked genes. Taken together the data indicate that Cbx1 is an HP1 ortholog and is likely to function in the recognition of H3K9me2/3 in *Z. tritici.*

Deletion of *cbx1* and *kmt1* results in distinct effects on growth *in vitro* and *in planta*.

The role of HP1 in the fitness of *Z. tritici* was investigated by generating *cbx1* deletion strains. For comparison, we also constructed strains lacking the H3K9 methyltransferase gene, *kmt1* and confirmed the loss of H3K9me3 marks in these mutants (Fig S1A). Initially, the *in vitro* growth and stress-sensitivity profiles of the Δ*cbx1* and Δ*kmt1* mutants relative to the IPO323 reference strain were determined. As previously reported, deletion of *kmt1* resulted in a slow growth phenotype (Möller *et al.*, 2019) but surprisingly, the Δ*cbx1* strains showed no marked reduction in fitness (Fig 3). Furthermore, although Δ*kmt1* strains were sensitive to osmotic stresses (NaCl, sorbitol), oxidative stress (H_2O_2) and cell wall damaging agents (Calcofluor and Congo Red) loss of *cbx1* did not result increase the sensitivity of *Z. tritici* to any of these

agents. However, we did note that Δ*cbx1* strains exhibited a slight increase in sensitivity to hydroxyurea which results in reduced dNTP levels and replication stress. Deletion of *cbx1* also resulted in increased levels of melanisation on PD agar (PDA) at 25°C (Fig. 3).

Loss of Kmt1-mediated H3K9 methylation is associated with a severe reduction in virulence (Möller *et al.*, 2019) and this was confirmed using our Δ*kmt1* strains (Fig S1B). To determine if Cbx1 is required for the pathogenicity of *Z. tritici*, wheat infection assays were carried out with the Δ*cbx1* strains. Disease symptoms presented in leaves treated with both the reference (IPO323) and Δ*cbx1* strains, but the onset of symptoms was delayed in the latter (Fig 4A). This was apparent at 14 days post inoculation (dpi) where the areas of leaf covered by necrotic lesions were reduced in the leaves treated with Δ*cbx1* mutants (Fig 4A). Furthermore, at 21 dpi, which typically marks the endpoint of infection, Δ*cbx1* treated leaves had a reduction in the number of visible pycnidia present on the leaf (Fig 4B & C). Therefore, removal of the HP1 homolog Cbx1 results in reduced virulence, but it does not abolish virulence as is the case for the loss of Kmt1. As such the deletion of *cbx1* does not phenocopy the loss of *kmt1* suggesting that H3K9me marks do not exclusively mediate their downstream biological effects through the recruitment of Cbx1.

Cbx1 and Kmt1 regulate the expression of overlapping sets of genes

To further understand the relationship between Cbx1 and Kmt1, their impacts upon the transcriptome were determined using RNA-seq analysis. RNA was analysed from two biological replicates of two independent isolates of Δ*cbx1* and we also sequenced RNA from two biological replicates of a Δ*kmt1* mutant and the reference IPO323 strain. Principal component analysis revealed a clear grouping of samples from the Δ*cbx1*

187 isolates and the biological replicates for all strains, indicative of low variation (Fig S2).
188 Next, hierarchical clustering was employed to provide an overview of the global
189 similarities between the transcriptomes of the sequenced strains. This revealed that
190 the transcript profiles of Δ*cbx1* and Δ*kmt1* mutants exhibit an overall similarity. Indeed,
191 the Δ*cbx1* mutant profiles were found to be more similar to the Δ*kmt1* strain than to
192 the reference strain (Fig 5A).

193 The transcriptomes of Δ*cbx1* and Δ*kmt1* mutant strains were further analysed
194 by identification of differentially expressed (DE) transcripts from protein coding genes
195 with DEseq2 ($p < 0.05$) (Love *et al.*, 2014). Global trends in gene expression were
196 visualised using MA plots (Δ*cbx1* vs IPO322 and Δ*kmt1* vs IPO323) (Fig 5B & C). As
197 expected based on previous analysis (Möller *et al.*, 2019), the majority of DE
198 transcripts in Δ*kmt1* were upregulated and the Δ*cbx1* DE transcripts also exhibited a
199 similar trend. Furthermore, for both strains the majority of down-regulated transcripts
200 showed a relatively modest (2-5 fold) decrease in abundance. In comparison, a greater
201 proportion of upregulated transcripts exhibited a more marked (5-10 fold) change in
202 levels. Therefore, like Kmt1, the HP1 protein Cbx1 plays an important role in gene
203 silencing in *Z. tritici*.

204 Genes that were differentially expressed in the Δ*kmt1* and Δ*cbx1* backgrounds
205 were filtered to select only those that exhibited at least a two-fold change in
206 expression. The total number of DE genes in this category in Δ*cbx1* and Δ*kmt1* was
207 1157 and 1291 respectively (Tables S1 and S2). Of these genes, 813 were
208 differentially expressed in both strains, an overlap which was found to be highly
209 significant (Fig 5D). The lists of DE genes were further filtered to distinguish between
210 up- and down-regulated genes. Significant overlaps between Δ*cbx1* and Δ*kmt1* gene
211 lists were observed in both categories (Fig 5E & F). Nonetheless, we did identify genes

that were differentially expressed in Δ*cbx1* but not Δ*kmt1* and vice versa (Table S3 and S4). The existence of these non-overlapping sets of DE genes may, at least in part, explain the differences in the phenotypes associated with Δ*cbx1* and Δ*kmt1* mutants.

The similarity of the RNA-seq data from the Δ*kmt1* strain generated in this study and the Zt09-Δ*kmt1* strain (Möller *et al.*, 2019) was also analysed. For this comparison the more stringent cut-offs (4-fold change in expression, adjusted p value < 0.001) employed by Moller *et al*. were used. Despite the potential for differences in strain background and experimental variability, the overlap in DE genes was highly significant and indicative of a high degree of similarity between the Δ*kmt1* mutant analysed in this study and Zt09-Δ*kmt1* (Fig S3). To determine whether increased stringency affected the relationship between Δ*cbx1* and Δ*kmt1* DE genes, the comparison was repeated using the 4-fold change cut-off. This analysis also revealed a highly significant overlap in the DE gene lists ($p < 0.001$; Fisher's test). Overall, these findings indicate that Cbx1 and Kmt1 regulate the expression of similar, albeit non identical, sets of protein-coding genes and are therefore consistent with Cbx1 playing a major role in the function of H3Kme2/3 marks in *Z. tritici.*

Loss of Cbx1 does not result in a global increase in expression from accessory chromosomes or TEs

It has been demonstrated that deletion of *kmt1* results in a global increase in transcripts derived from the heterochromatin- and TE-enriched accessory chromosomes (Möller *et al.*, 2019). To determine whether this was also the case for mutants lacking *cbx1*, normalised read counts were mapped from genes on accessory chromosomes. As expected a significant increase in read counts from accessory

chromosomes was observed in the Δ*kmt1* mutant compared to IPO323 ($p < 0.014$; ANOVA). In contrast no significant increase ($p < 0.29$; ANOVA) was observed in the Δ*cbx1* background (Fig 6A). Therefore, loss of Cbx1 is not sufficient for a global increase in expression from genes on accessory chromosomes.

The accessory chromosomes of *Z. tritici* are highly enriched in TEs and previously it has been shown that expression from these elements is suppressed by H3K9me2/3 (Möller *et al.*, 2019). We therefore determined the effect of Cbx1 on the global level of transcripts derived from TEs. As previously observed (Möller *et al.*, 2019), a significant net increase in the expression of TEs was detected in Δ*kmt1* ($p <$ 8.25e-09 ANOVA), however in contrast, no significant global increase the Δ*cbx1* mutant was detected (Fig 6B). Indeed, hierarchical clustering revealed that with respect to the profile of TE expression, the Δ*cbx1* mutant is more similar to the reference IPO323 strain than to the Δ*kmt1* mutant (Fig 6C). Therefore, although global silencing of TEs in *Z. tritici* requires Kmt1, and by implication H3K9me2/3, it is not dependent upon recognition of these histone modifications by the HP1 protein, Cbx1.

Cbx1 regulates the expression of a significant proportion of TE-associated genes

An increased frequency of recombination is often observed around loci surrounding TEs. Genetic instability around such loci in filamentous fungi has been proposed to drive rapid evolution and aid niche adaptation (Dong *et al.*, 2015, Faino *et al.*, 2016, Laurent *et al.*, 2018). Therefore, we analysed the expression of all genes within 2 kb of a TE. In total 1505 genes were identified as 'TE-associated' of which 184 were differentially expressed in Δ*cbx1* and 205 in Δ*kmt1*, a highly significant enrichment in both cases ($p <$ 4.35e-07 and $p <$ 9.66e-08 respectively). Furthermore, 114 TE-

associated genes were found to be commonly differentially expressed in Δ*cbx1* and Δ*kmt1* ($p < 5.55e-65$) (Fig 6D). The expression profile of these genes was also found to be highly similar between the Δ*cbx1* and Δ*kmt1* mutants and indeed all but 4 genes exhibited similar expression patterns (Fig 6E). GO-term analysis of the differentially expressed TE–associated genes revealed that 8 of the 114 were annotated as having functions relating to secondary metabolism. However, the majority of these were 'orphan' genes with no assigned GO terms. This is not unexpected given that TE-associated and heterochromatic loci are known to be enriched with 'orphan' genes in a variety of plant pathogenic fungi (Dong *et al.*, 2015).

Protein encoding genes that are differentially expressed in Δ*cbx1* exhibit only a weak correlation with H3K9me

The removal of HP1 tends to result in the upregulation of genes that are associated with H3K9me2/3-marked chromatin (Chujo & Scott, 2014, Reyes-Dominguez *et al.*, 2010, Soyer *et al.*, 2014). To investigate whether this is the case in *Z. tritici*, genes that were partially (>1 bp) or completely associated with H3K9me were identified through analysis of published ChIP-seq data (Schotanus *et al.*, 2015). The relationship between H3K9me-associated genes and genes that are differentially expressed in Δ*cbx1* was then determined. A total of 247 genes were found to be partially associated with H3K9me (>1 bp) while only 112 were completely associated with this modification. Of the partially H3K9me-associated genes only 31 were differentially expressed in Δ*cbx1*, an overlap which was just statistically significant ($p < 0.023$) (Fig 7A). The overlap between the completely H3K9me-associated genes and Δ*cbx1* DE genes was also modest (17 genes, $p < 0.016$) (Fig 7B). At first glance this weak correlation is surprising, however it has previously been observed that

deletion of *kmt1* is not sufficient for the upregulation of the majority of H3K9me-associated genes in *Z. tritici* (Möller *et al.*, 2019) and analysis of the Δ*kmt1* RNA-seq data generated in this was consistent with these findings. Only a very modest overlap was observed between Δ*kmt1* DE genes and genes that are fully associated with H3K9me and no significant overlap was observed with partially associated genes (Fig 7C & D). Overall, only a very small number of protein coding genes are located in H3K9me-marked chromatin in *Z. tritici* and under *in vitro* growth conditions, the disruption of heterochromatin is insufficient to activate their expression.

Cbx2, a fungal-specific CD protein that binds to H3K9me3.

Comparison of the phenotypes of Δ*kmt1* and Δ*cbx1* mutants suggested that some of the downstream effects of H3K9me2/3 histone modifications are likely to be mediated independently of the HP1 homolog Cbx1. One explanation for this would be that *Z. tritci* has additional H3K9me2/3 reader proteins. Therefore, we used BLAST analyses to search for further proteins with the potential to bind H3K9me2/3 PTMs and identified five hypothetical proteins with CD domains (as predicted by ExPASy Prosite and or Pfam). None of these proteins contained a recognisable CSD, consistent with Cbx1 being the sole HP1 isoform in *Z. tritici*. Four of the hypothetical CD proteins were eliminated from further analysis for one or more of the following reasons, (i) they exhibited similarity to retroviral/retrotransposon integrases, (ii) the CD domain lacked critical key aromatic methyl-lysine caging residues or (iii) they were encoded on an accessory chromosome. The remaining hypothetical protein (Mycgr3G108849, hereafter called Cbx2) was predicted to be 703 amino acids in length and have two CD domains in the C-terminal region (Fig 8A and Fig S4). BLAST analyses revealed that organisms that encode proteins with homology to Cbx2 extending beyond the CD

312 domains are limited to species in just a few fungal families (principally the
313 *Mycosphaerellaceae* and *Teratosphaeriaceae*) (Fig 8B and Fig S5). Therefore, unlike
314 the broadly conserved HP1 family member Cbx1, Cbx2 is a fungal-specific CD protein.
315 Sequence analysis revealed that both Cbx2 CDs possess the conserved
316 'aromatic cage' residues that facilitate methyl-lysine binding (Fig S4) and furthermore,
317 chromodomain 1 (CD1) was predicted to be acidic, a characteristic of HP1-type
318 H3K9me binding proteins (Hiragami-Hamada & Nakayama, 2019). Therefore, we
319 investigated the histone binding preferences of Cbx2. A region that encompassed both
320 CD domains (amino acids 503 to 703), was expressed as a GST fusion protein in *E.*
321 *coli* and purified. Pull-down assays indicated that this domain of Cbx2 binds to histone
322 H3 peptides that are methylated at lysine 9. However, Cbx2 exhibited a clear
323 preference for H3K9me3 relative to H3K9me2 and no specificity for any other tested
324 modification was observed (Fig 8C & D).
325 The histone peptide binding assays suggested that Cbx2 has the potential to
326 function as an effector of H3K9me3 PTMs and so Δ*cbx2* strains were generated.
327 Comparison of the Δ*cbx2* mutant with the IPO323 reference strain indicated that loss
328 of Cbx2 does not result in any detectable reduction in fitness or stress resistance (Fig
329 S6). Furthermore, wheat infection assays revealed that, unlike the Δ*kmt1* and Δ*cbx1*
330 strains, Δ*cbx2* strains exhibited no obvious reduction in virulence (Fig 9A and B).
331 Leaves treated with Δ*cbx2* mutants developed disease symptoms at a very similar rate
332 to those treated with the reference IPO323 strain and there was no major difference
333 in the numbers of pycnidia at 21 dpi (Fig 9C). As such, loss of Cbx2 alone does not
334 obviously impact the growth of *Z. tritici* either *in vitro* or *in planta*. This is perhaps not
335 surprising, as when we analysed the expression of *cbx2* using our RNA seq data, we

found that this gene was expressed at similar levels to the H3K9 methyltransferase *kmt1*, but at only ~2.9% of the level of *cbx1*.

We hypothesized that Cbx2 may co-operate with Cbx1 but that effects of *cbx2* deletion may be masked when *cbx1* is present. As a test of this, a double deletion mutant was constructed by inserting a *neo* resistance cassette into the *cbx1* locus in the Δ*cbx2* background. Importantly, analysis of the fitness and stress sensitivity profiles of these strains showed that the Δ*cbx1* Δ*cbx2* double mutant has *in vitro* growth phenotypes that closely resemble those associated with Δ*kmt1.* Like the Δ*kmt1* strains, Δ*cbx1* Δ*cbx2* double mutant strains had a slow growth phenotype and were sensitive to osmotic stress (NaCl), oxidative stress (H_2O_2), cell wall damaging agents (Calcofluor and Congo Red) and genotoxic agents (HU and Bleomycin) (Fig 10A). As such the deletion of *cbx1* and *cbx2* in combination mimics the loss of H3K9me. These results are consistent with a model whereby key functions of H3K9me PTMs are mediated by a combination of the HP1 homolog Cbx1 and the fungal-specific chromodomain protein, Cbx2.

The phenotypes of the Δ*cbx1* Δ*cbx2* double mutant, suggested that Cbx1 and Cbx2 may have redundant functions in gene silencing. We therefore analysed some Kmt1-repressed genes whose expression is not de-repressed by deletion of *cbx1* alone (Fig 5E and Table S4). RT-qPCR analysis showed that the expression of one such Kmt1-repressed gene (*Mycgr3G103556*) was only marginally increased in the Δ*cbx1* Δ*cbx2* double mutant (Fig 10B). In contrast, the deletion of both *cbx1* and *cbx2* genes in combination resulted in an increase in expression of *Mycgr3G44980* comparable to the Δ*kmt1* strain (Fig 10C). Therefore, Cbx1 and Cbx2 do function redundantly to silence the expression of some Kmt1-regulated Z. *tritici* genes.

DISCUSSION

Heterochromatic H3K9me histone modifications, have a major impact upon the chromosomal stability and virulence of *Z. tritici* (Möller *et al.*, 2019). Here we have identified two chromodomain proteins, Cbx1 and Cbx2, which recognize these marks and are implicated in mediating downstream biological events.

Cbx1 bears all the hallmarks of an HP1 ortholog, as it binds to H3K9me2/3 *in vitro* and is enriched at heterochromatic loci. Furthermore, Cbx1 and the H3K9 methyltransferase, Kmt1, regulate the expression of overlapping sets of protein encoding genes. Recognition of H3K9me2/3 modifications by HP1 proteins constitutes a fundamentally conserved step in the formation and function of heterochromatin (Kumar & Kono, 2020). This central role is illustrated by the finding that in some species, such as fission yeast, the phenotypes associated with the loss of HP1 proteins and the respective histone H3K9 methyltransferase are highly similar (Allshire *et al.*, 1995). Despite Cbx1 being the sole HP1 homolog in *Z. tritici*, Δ*cbx1* strains have *in vitro* and *in planta* growth defects that are less severe than Δ*kmt1* mutants. These findings are consistent with the data from other plant-associated fungi such as *E. festucae*. While both HepA (HP1) and ClrD (H3K9 methyltransferase) are required for the symbiotic mutualist interaction of *E. festucae* with the grass *Lolium perenne*, Δ*hepA* mutants have only mild defects in axenic culture in comparison to strains lacking Δ*clrD* (Chujo *et al.*, 2019). Also RNAi silencing of the HP1 and H3K9 methyltransferase homologs has different effects on the virulence of the oil seed rape pathogen, *L. maculans* (Soyer et al., 2014). It is possible that there are additional H3K9me readers in these organisms.

The transcriptomic analysis revealed a highly significant overlap in the differentially expressed genes in the Δ*kmt1* and Δ*cbx1* backgrounds. Nonetheless, a

set of genes was identified whose expression was dependent upon Cbx1, but independent of Kmt1 (Table S3). This suggests that Cbx1 has functions that are independent of H3K9me2/3. Consistent with this, H3K9me-independent roles for HP1 isoforms at telomeres and in DNA damage responses have been reported (Zeng *et al.*, 2010). Furthermore, it is well recognised that individual HP1 proteins can be functionally promiscuous and have variety of roles outside of heterochromatin, including transcriptional activation (Zeng *et al.*, 2010).

Analysis of the genomic distribution of H3K9me marks in *Z. tritici* has demonstrated that these modifications are predominantly associated with TE elements (Möller *et al.*, 2019). Deletion of *kmt1* is associated with a global increase in the abundance of transposon-derived transcripts (Möller *et al.*, 2019), a finding that was confirmed in this study. Therefore, in *Z. tritici* as in other eukaryotes, heterochromatin represents a key mechanism for suppressing the activity of repetitive elements. Surprisingly, our findings suggest that Cbx1 is dispensable for the restriction of these elements, at least at a global level and only a small number of TEs are differentially expressed in the Δ*cbx1* strain. *Z. tritici* has up to eight accessory chromosomes that are highly enriched with TEs and are proposed to provide a selective advantage under some environmental conditions (Habig *et al.*, 2017). Loss of Kmt1 is associated with a global activation of TEs, elevated loss of accessory chromosomes and wide scale genome rearrangements. The genomic instability in Δ*kmt1* mutants is driven by the redistribution of H3K27me3 modifications which invade regions previously occupied by H3K9me2/3 (Möller *et al.*, 2019). That removal of Cbx1 does not result in a global increase in transcripts derived from either TEs or accessory chromosomes, suggests that HP1 function may not be necessary to prevent wide scale re-localization of H3K27me3 modifications. While the loss of H3K9me2/3 severely impacts the ability of

411 *Z. tritici* to colonize wheat leaves, this does not seem to result from mitotic instability
412 as deletion of the H3K27 methyltransferase gene *kmt6* in the Δ*kmt1* background
413 suppresses the elevated level of accessory chromosome loss but does not rescue
414 virulence (Möller *et al.*, 2019).

415 The non-identical phenotypes of the Δ*kmt1* and Δ*cbx1* mutants suggested that
416 additional readers of H3K9me2/3 marks are present in *Z. tritici*. Consistent with this
417 prediction, we have identified Cbx2, a chromodomain protein that recognises
418 H3K9me3 *in vitro*. Unlike Cbx1, which is an HP1 family member and is thus broadly
419 conserved, Cbx2 homologs are restricted to some dothideomycete species suggesting
420 a specialised role in heterochromatin assembly and or maintenance. Also, preliminary
421 evidence suggests that Cbx2 is much less abundant than Cbx1. The *in vitro* binding
422 studies also indicated that the Cbx2 CD region had a preference for H3K9me3 relative
423 to H3K9me2. This is potentially important as analysis of these marks in *S. pombe* has
424 revealed that they demarcate functionally distinct types of heterochromatin that recruit
425 reader proteins with different efficiencies and have different transcriptional silencing
426 potential (Jih *et al.*, 2017).

427 Cbx2 has an unusual structure in that it contains two closely related
428 chromodomains (CD1 and CD2). So far the only characterised proteins that have a
429 double chromodomain structure are the CHD (chromo-ATPase/helicase-DNA-binding)
430 proteins that belong to the SWI/SNF superfamily of ATP-dependent chromatin
431 remodelling enzymes (Yap & Zhou, 2011). It should be noted that the CHD
432 chromodomains belong to a distinct clade that is not involved in the recognition of
433 heterochromatic marks (Yap & Zhou, 2011). The sequences of the Cbx2 CDs are
434 closely related suggesting they arose by duplication. In support of this, some species
435 (e.g. *Polychaeton citri, Ramularia collo-cygni* and *Acidomyces richmondensis*) have

436 Cbx2 homologs that have only a single CD (Fig 8B and Fig S5). It is not yet clear how
437 Cbx2 binds H3K9me3 but it is tempting to suggest that it is achieved via CD1. CD1 is
438 acidic and is flanked by acidic upstream and basic downstream regions,
439 characteristics of H3K9me-binding chromodomains (Hiragami-Hamada & Nakayama,
440 2019).

441 While our results suggest that both Cbx1 and Cbx2 are important in executing
442 the functions of H3K9me marks, it is possible that some aspects of their biological
443 function are independent of methyl-lysine reader proteins. Indeed, methylation of
444 lysine 9 may influence transcription or other aspects of chromatin function by
445 preventing the acetylation of this residue. It is also possible that Kmt1 may mediate
446 some functions through the methylation of non-histone targets as has been
447 documented for other SET domain histone methyltransferases (Carlson & Gozani,
448 2016).

449 Only a small number of protein encoding genes are located in H3K9me-marked
450 chromatin in *Z. tritici* and consistent with previous findings only a fraction of these
451 genes are differentially expressed in the Δ*kmt1* and Δ*cbx1* mutants. However, analysis
452 of DE genes in Δ*kmt1* has revealed a significant enrichment for genes located in the
453 vicinity of TEs and similar relationship was also observed for Δ*cbx1*. These findings
454 suggest that the heterochromatin associated with TEs can shape the expression of
455 genes in the surrounding chromosomal loci. Indeed, the ability of TE insertions to
456 impact the expression of adjacent genes in *Z. tritici* has been demonstrated (Krishnan
457 *et al.*, 2018). It is also noteworthy that *Drosophila* HP1a binds to promoters
458 independently of H3K9me marks and it has been proposed that HP1a then makes
459 transient looping contacts with H3K9me target sites in surrounding regions (Figueiredo
460 *et al.*, 2012). This model may explain how H3K9me-marked TEs influence the

461 expression of nearby genes in *Z. tritici*. Furthermore, TEs have been implicated in the
462 organization of loops and other higher order chromosomal structures in a variety of
463 species including fission yeast, flies, plants and mammals (Cam *et al.*, 2008,
464 Choudhary *et al.*, 2020, Mamillapalli *et al.*, 2013, Sun *et al.*, 2020).

465 Analysis of the genomes of fungal phytopathogens has revealed that effector
466 genes tend to be associated with rapidly evolving regions of the genome that are
467 associated with repetitive elements (Dong *et al.*, 2015). These observations have led
468 to the suggestion that repetitive elements may organize the regions of genome into
469 functional compartments that drive adaptive evolution. Therefore, it is interesting that
470 the expression of a significant proportion of TE-associated genes is influenced by
471 Kmt1 and Cbx1. Furthermore, recent analysis indicates that genes that are highly
472 expressed at the switch of *Z. tritici* to necrotrophic growth during infection are amongst
473 those most upregulated in the absence of Kmt1 (Soyer *et al.*, 2019). Therefore, it will
474 be important to determine how Cbx proteins and the reprogramming of H3K9me-
475 dependent heterochromatin structures contribute to changes in transcriptional
476 programmes during plant infection.

EXPERIMENTAL PROCEDURES

Strains, Media and Plasmids

Zymoseptoria tritici strains were cultivated on YMS medium (0.4% [w/v] yeast extract, 0.4% [w/v] malt extract, 0.4% [w/v] sucrose) at 18˚C in a shaking incubator at 200 rpm. When solid medium was required Bacto agar was added at 2% [w/v]. Gene deletion strains were constructed using *Agrobacterium tumefaciens*-mediated transformations of IPO323 using plasmids derived from pCHYG as previously described (Motteram *et al.*, 2009). Flanking regions (>1kb) of the targeted gene were PCR amplified and introduced into pCHYG by Gibson assembly. Gene deletions of *kmt1*, *cbx1* and *cbx2* were constructed by insertion of a hygromycin resistance cassette (*hph*) into the desired locus. The *cbx1 cbx2* double deletion mutant was constructed by inserting a G418 resistance cassette (*neo*) into the *cbx1* locus in the *cbx2* deletion mutant. Correct integration was confirmed by PCR genotyping. Plasmid pCGEN-YR-*cbx1GFP* was constructed by introducing fragments consisting of the *cbx1* promoter, the *cbx1* ORF fused to *EGFP* and 1 kb of terminator sequence from the β-tubulin gene into the *BamHI* site of pC-G418-YR (Sidhu *et al.*, 2015) using recombinational cloning in *Saccharomyces cerevisiae*. For the assessment of growth *in planta*, wheat infection assays were performed as previously described (Keon *et al.*, 2007).

In vitro sensitivity assays

Z. tritici strains were cultured on YMS agar plates for 7 days at 18°C. Cells were then harvested, washed once in sterile 1 x PBS and diluted to OD_{600} of 1.0. Cells were subjected to five-fold serial dilution and pinned onto the indicated YMS and PD agar (Formedium) plates with a 48-pin tool (Sigma). UV irradiation was achieved using a

Stratalinker 2400 UV crosslinker (Stratagene). Plates were then incubated for 7 days at 18°C unless otherwise indicated.

GST fusion proteins

Recombinant Cbx1 was expressed fused to an N-terminal Glutathione-S-Transferase (GST) tag. The *cbx1* sequence (codon optimised for *E. coli*) was synthesized (Eurofins Genomics), cloned into pGEX-6P-1 and transformed in *E. coli* (BL21). Transformants were grown in 2L of LB at 37˚C until an OD_{600} of 0.5-0.6 was reached, IPTG was add to a final concentration of 0.5 mM and the culture was incubated at 18˚C for 16 hours. The cells were harvested by centrifugation and the resulting pellet was resuspended in 50 mL lysis buffer (50 mM Tris HCl [pH 8.0] 500 mM NaCl 1 mM PMSF), snap frozen in liquid nitrogen and stored at -80. Thawed cell pellets were supplemented with an additional 1 mM PMSF and lysed using a One Shot homogeniser (Constant Systems Ltd) at 20 KPSI at 4˚C and then centrifuged at 19 000 RPM in a JA-25.50 rotor (Beckman Coulter) for 30 minutes at 4˚C. The supernatant was incubated with 500 µL Pierce™ Glutathione Agarose (Thermo Scientific) pre-equilibrated in wash buffer (50 mM Tris HCl [pH 8.0] 500 mM NaCl) on a rotator for 1 hour. The lysate was then centrifuged at 700 x *g* for 2 minutes and the supernatant discarded. The glutathione agarose was washed once, resuspended in 10 mL wash buffer and applied to a 10 mL disposable gravity flow column (Thermo Scientific). The agarose resin was then washed until a basline A_{280} value was reached. GST fusion protein was eluted off the column in 1 mL fractions using wash buffer supplemented with 10 mM glutathione. Fractions containing GST-Cbx1 were pooled and then subjected to size exclusion chromatography using a Superdex 200 column (GE Lifesciences).

Recombinant GST-Cbx2, composed of an N-terminal GST tag fused to the C-terminal 22 kDa of Cbx2 (amino acids 503 to 703) was produced by Dundee Cell Products.

Histone H3 peptide binding assays

1 µg of GST tagged protein was added to 1 µg of biotin labelled peptide (EpiCypher) in 300 µL pulldown binding buffer (50 mM Tris [pH 7.5], 300 mM NaCl, 0.01 % NP-40) and rotated overnight at 4˚C on a rotating wheel. An aliquot (30 µL) of a 50 % slurry of streptavidin beads (Thermo Scientific) pre-equilibrated in pulldown binding buffer, was added and the sample and incubated at 4°C for one hour on a rotating wheel. Beads were then pelleted by centrifugation at 800 x g for 1 minute and washed four times with 1 mL pulldown binding buffer. The supernatant was removed and streptavidin beads were boiled in 60 µL 2 x protein loading dye (125 mM Tris-HCL [pH 6.8], 20 % glycerol [v/v], 5 % SDS [w/v], 370 mM β-mercaptoethanol [added directly before use]). A control sample of GST fusion protein (100 ng) was loaded alongside the pulldown samples which were resolved on 10% SDS polyacrylamide gels and subject to western blotting using anti-GST antibody (Sigma G7781). Membranes were developed with an ECL plus Chemiluminescent kit (GE Healthcare) and imaged on a Typhoon FLA 9500 (GE Healthcare). GST fusion protein levels relative to the input control were quantified using image J.

Chromatin Immunoprecipitation (ChIP) Assays

An exponential phase culture of *Z. tritici* was diluted to OD_{600} 0.25, grown overnight at 18°C, and harvested at OD_{600} 0.80. For each 100 mL of culture, 1.35 mL 37 % formaldehyde (Sigma Aldrich) was added to each flask and the cells fixed for 15 minutes. 2 mL 2.5 M glycine was then added to quench the remaining formaldehyde

and the flasks incubated at room temperature for a further 5 minutes. Cells were harvested by centrifugation and washed sequentially in 50 mL and 2 mL sterile MilliQ water. Cell pellets were snap-frozen in liquid nitrogen and stored at -80°C. Tissue was ground in under liquid nitrogen in a pestle and mortar and resuspended in freshly made chromatin buffer (50 mM HEPES [pH7.5], 20 mM NaCl, 1 mM EDTA, 1 % Triton X-100, 0.1 % sodium deoxycholate [w/v]) supplemented with protease inhibitors (1 mM PMSF, 1 µg/mL leupeptin, 1 µg/mL E-64, 0.1 µg/mL pepstatin). $CaCl_2$ was then added to a final concentration of 2 mM. To initiate digestion, 150 U MNase (USB/Pharmacia) (prepared as 15 U/µL in 10 mM Tris HCl [pH7.5] 10 mM NaCl 100 µg/ml BSA) per 1 mL of lysate was added and the reaction incubated at 37°C for 20 minutes with frequent mixing by inversion of the tubes. Digestion was stopped by the addition of EGTA to a final concentration of 2 mM. The cell debris was pelleted at 4000 rpm at 4 °C in a microcentrifuge centrifuge and the supernatant was retained. Two 100 µL aliquots of the lysate were taken to be used as 'input' and to check MNase digestion respectively. The remaining lysate split was into 200 µL fractions to be used in each immunoprecipitation. To each IP fraction 2 µL of α-GFP antibody (A-11122 – Invitrogen) was added and incubated rotating overnight at 4°C. The following day, 20 µL protein A Dynabeads® (Invitrogen), pre-equilibrated in chromatin buffer were added to each IP and rotated at 4 °C for 2 hours. The supernatant was then removed, and the beads washed twice for 5 minutes at 4 °C in ChIP lysis buffer (50 mM HEPES [pH 7.4], 140 mM NaCl, 1 mM EDTA [8.0], 1 % Triton X-100 [v/v], 0.01 % sodium deoxycholate [w/v]). The beads were then washed once in each of the following buffers: ChIP lysis buffer + 500 mM NaCl, LiCl buffer (10 mM Tris-HCl [pH 8.0], 250 mM LiCl, 0.5% NP40 [v/v], 0.5 % sodium deoxycholate [w/v], 1 mM EDTA), TE buffer (10 mM TRIS [pH 8.0], 1 mM EDTA [pH 8.0]) On the final wash the supernatant was

575 removed and 100 µL 10 % Chelex® 100 (w/v) (Bio-Rad) in MilliQ water was added the
576 beads. 100 µL of 10% Chelex® 100 (w/v) was also added to 10 µL of the input fraction.
577 All samples were then boiled at 100°C for 12 minutes. 2.5 µL 10 mg/mL proteinase K
578 was then added, and the samples incubated at 55°C for 30 minutes. Samples were
579 then boiled at 100°C for 10 minutes, after which the beads and Chelex® were pelleted
580 and 60 µL of the supernatant transferred to a clean tube. The input and IP fractions
581 were diluted by 1:000 and 1:5, respectively. 2 µL of diluted input and IP template were
582 used for each 10 µL qPCR reaction. qPCR was carried out with a KAPA SYBR® FAST
583 qPCR Master Mix Kit with 0.2 mM forward and reverse primers in a Rotor-Gene® 6000
584 HRM Real Time PCR Machine (Corbett). Primer sequences are detailed in Table S5.
585
586 **RNA extraction**
587 Dense liquid cultures of *Z. tritici* were diluted to 0.1 OD_{600} in fresh YMS and grown
588 to OD_{600} 1.0. Cells were then harvested, snap frozen in liquid nitrogen and ground to
589 a fine powder in liquid nitrogen with a pestle and mortar. Approximately 100 mg of
590 ground tissue was added to 2 mL of Tri reagent (Invitrogen), transferred to a 2 mL
591 heavy lock tube (Eppendorf) and centrifuged at 16 000 x g for 5 minutes. The
592 supernatant was extracted with chloroform/isoamyl alcohol and then RNA was
593 precipitated by the addition of an equal volume of propan-2-ol, followed by
594 centrifugation at 16 000 x g for up to 30 minutes. The pellet was washed twice in 70%
595 ethanol, air dried for 15 minutes at room temperature and resuspended in
596 50 uL of MilliQ water. Aliquots were stored at -80˚C until required. For RNA
597 sequencing experiments samples were purified using an RNA Clean and Concentrate
598 column (Zymo research) according to the manufacturer's instructions.
599

600 **RT-qPCR**

601 RNA to be reverse transcribed to cDNA was first treated with Precision DNase (Primer
602 Design) following the manufacturer's instructions. cDNA was then prepared using
603 SuperScript™ IV Reverse Transcriptase (Invitrogen) with Random Hexamers
604 (Invitrogen) following the manufacturer's instructions. qPCR was carried out with as
605 described for ChIP assays. Primer sequences are detailed in Table S5.

606

607 **RNA-seq and bioinformatics**

608 Purified RNA samples were sequenced by Novogene (China). Read quality was
609 confirmed by FastQC version 0.11.9 (Andrews, 2010) and MultiQC version 1.8 (Ewels
610 *et al.*, 2016). STAR version 2.7.1a (Dobin *et al.*, 2013) was used to index and align
611 reads to the MG2 IPO323 genome assembly. 'FeatureCounts' version 1.6.5 from the
612 Subread package (Liao *et al.*, 2014) was used to count reads mapped to genes. Gene
613 annotations (King *et al.*, 2017) was used for alignment and read counting. File
614 conversions and manipulations were carried out with SAMtools (Li *et al.*, 2009) and
615 BAMtools (Barnett *et al.*, 2011). Where necessary BEDTools (Quinlan, 2014) was
616 used to convert between the Zt09 (an IPO323 derivative strain) gene annotation
617 (Grandaubert *et al.*, 2015) and the IPO323 strain annotation (King *et al.*, 2017).
618 Mapping of reads to transposable elements followed the same analysis pipeline using
619 transposable element annotation (Grandaubert *et al.*, 2015). To minimise differences
620 caused by data analysis, published ChIP-seq data (Schotanus *et al.*, 2015) was
621 analysed following the previously described workflow (Schotanus *et al.*, 2015) with
622 minor modifications including read trimming using Trimmomatic (Bolger *et al.*, 2014),
623 alignment with Bowtie 2 version 2.4.1 (Langmead & Salzberg, 2012) and peak
624 coverage determined by RSEG version 0.4.9 (Song & Smith, 2011). Peaks that

625 occurred in both replicates were merged using BEDTools. Gene annotations (King *et*
626 *al.*, 2017) were merged with bed files of identified ChIP-seq peaks to generate lists of
627 genes marked by the specified histone modification (completely or < 1 bp association).
628 Read counts were imported into R, normalised and subject to differential expression
629 analysis with DESeq2 (Love *et al.*, 2014). DESeq2 was run independently for protein
630 coding genes and transposable elements. Data manipulation and data plotting were
631 carried out in R with the dplyr, stringr, and ggplot2 packages from the tidyverse
632 (Wickham *et al.*, 2019) and the reshape2 package (Wickham, 2007). Heatmaps were
633 made in R with pheatmap (Kolde, 2019). Eggnog mapper (Huerta-Cepas *et al.*, 2017)
634 was run to gain additional functional information for the differentially expressed genes.
635

636 **DATA AVAILABILITY**

637 The sequence data that support the findings of this study are available at the NCBI
638 Sequence Read Archive (SRA) under accession PRJNA769830. Additional sequence
639 data were derived from resources available in the public domain at the SRA under
640 accessions SRP059394 and PRJNA494102. Other data that support the findings of
641 this study are available from the corresponding author upon reasonable request.
642

643 **ACKNOWLEDGEMENTS**

644 We thank Elizabeth Veal for comments on the manuscript. CJF was supported by a
645 BBSRC NLD Doctoral Training Partnership studentship. The authors indicate no
646 conflict of interest.
647

648 **AUTHOR CONTRIBUTIONS**

649 CJF and SKW contributed to the conception and design of the study. All authors
650 contributed to the acquisition, analysis, and/or interpretation of the data and writing of
651 the manuscript.

652

653 **ABBREVIATED SUMMARY**

654 Heterochromatin associated with methylation of histone H3 on lysine 9 (H3K9me) is
655 required for the genome stability and virulence of the fungal pathogen, *Zymoseptoria*
656 *tritci.* We have identified chromodomain proteins, Cbx1 and Cbx2, which recognise
657 H3K9me and show that loss of these proteins mimics phenotypes that are associated
658 with the loss of the H3K9 methyltransferase, Kmt1. Overall, our data suggest that key
659 functions of H3K9me modifications are mediated by a combination of Cbx1 and Cbx2.

660 **REFERENCES**

661 Allshire, R.C., and Madhani, H.D. (2018) Ten principles of heterochromatin formation
662 and function. *Nat Rev Mol Cell Biol* **19**: 229-244.

663 Allshire, R.C., Nimmo, E.R., Ekwall, K., Javerzat, J.P., and Cranston, G. (1995)
664 Mutations derepressing silent centromeric domains in fission yeast disrupt
665 chromosome segregation. *Genes Dev* **9**: 218-233.

666 Andrews, S. (2010) FastQC: a quality control tool for high throughput sequence data
667 Available online at: http://www.bioinformatics.babraham.ac.uk/projects/fastqc.

668 Bannister, A.J., Zegerman, P., Partridge, J.F., Miska, E.A., Thomas, J.O., Allshire,
669 R.C., and Kouzarides, T. (2001) Selective recognition of methylated lysine 9 on
670 histone H3 by the HP1 chromo domain. *Nature* **410**: 120-124.

671 Barnett, D.W., Garrison, E.K., Quinlan, A.R., Stromberg, M.P., and Marth, G.T. (2011)
672 BamTools: a C++ API and toolkit for analyzing and managing BAM files.
673 *Bioinformatics* **27**: 1691-1692.

674 Bolger, A.M., Lohse, M., and Usadel, B. (2014) Trimmomatic: a flexible trimmer for
675 Illumina sequence data. *Bioinformatics* **30**: 2114-2120.

676 Cam, H.P., Noma, K., Ebina, H., Levin, H.L., and Grewal, S.I. (2008) Host genome
677 surveillance for retrotransposons by transposon-derived proteins. *Nature* **451**:
678 431-436.

679 Canzio, D., Larson, A., and Narlikar, G.J. (2014) Mechanisms of functional promiscuity
680 by HP1 proteins. *Trends Cell Biol* **24**: 377-386.

681 Carlson, S.M., and Gozani, O. (2016) Nonhistone Lysine Methylation in the Regulation
682 of Cancer Pathways. *Cold Spring Harb Perspect Med* **6**.

683 Choudhary, M.N., Friedman, R.Z., Wang, J.T., Jang, H.S., Zhuo, X., and Wang, T.
684 (2020) Co-opted transposons help perpetuate conserved higher-order
685 chromosomal structures. *Genome Biol* **21**: 16.
686 Chujo, T., Lukito, Y., Eaton, C.J., Dupont, P.Y., Johnson, L.J., Winter, D., Cox, M.P.,
687 and Scott, B. (2019) Complex epigenetic regulation of alkaloid biosynthesis and
688 host interaction by heterochromatin protein I in a fungal endophyte-plant
689 symbiosis. *Fungal Genet Biol* **125**: 71-83.
690 Chujo, T., and Scott, B. (2014) Histone H3K9 and H3K27 methylation regulates fungal
691 alkaloid biosynthesis in a fungal endophyte-plant symbiosis. *Mol Microbiol* **92**:
692 413-434.
693 Cowieson, N.P., Partridge, J.F., Allshire, R.C., and McLaughlin, P.J. (2000)
694 Dimerisation of a chromo shadow domain and distinctions from the
695 chromodomain as revealed by structural analysis. *Curr Biol* **10**: 517-525.
696 Dobin, A., Davis, C.A., Schlesinger, F., Drenkow, J., Zaleski, C., Jha, S., Batut, P.,
697 Chaisson, M., and Gingeras, T.R. (2013) STAR: ultrafast universal RNA-seq
698 aligner. *Bioinformatics* **29**: 15-21.
699 Dong, S., Raffaele, S., and Kamoun, S. (2015) The two-speed genomes of filamentous
700 pathogens: waltz with plants. *Curr Opin Genet Dev* **35**: 57-65.
701 Ewels, P., Magnusson, M., Lundin, S., and Kaller, M. (2016) MultiQC: summarize
702 analysis results for multiple tools and samples in a single report. *Bioinformatics*
703 **32**: 3047-3048.
704 Faino, L., Seidl, M.F., Shi-Kunne, X., Pauper, M., van den Berg, G.C., Wittenberg,
705 A.H., and Thomma, B.P. (2016) Transposons passively and actively contribute
706 to evolution of the two-speed genome of a fungal pathogen. *Genome Res* **26**:
707 1091-1100.

708 Figueiredo, M.L., Philip, P., Stenberg, P., and Larsson, J. (2012) HP1a recruitment to
709 promoters is independent of H3K9 methylation in Drosophila melanogaster.
710 *PLoS Genet* **8**: e1003061.
711 Goodwin, S.B., M'Barek S, B., Dhillon, B., Wittenberg, A.H., Crane, C.F., Hane, J.K.,
712 Foster, A.J., Van der Lee, T.A., Grimwood, J., Aerts, A., Antoniw, J., Bailey, A.,
713 Bluhm, B., Bowler, J., Bristow, J., van der Burgt, A., Canto-Canche, B.,
714 Churchill, A.C., Conde-Ferraez, L., Cools, H.J., Coutinho, P.M., Csukai, M.,
715 Dehal, P., De Wit, P., Donzelli, B., van de Geest, H.C., van Ham, R.C.,
716 Hammond-Kosack, K.E., Henrissat, B., Kilian, A., Kobayashi, A.K., Koopmann,
717 E., Kourmpetis, Y., Kuzniar, A., Lindquist, E., Lombard, V., Maliepaard, C.,
718 Martins, N., Mehrabi, R., Nap, J.P., Ponomarenko, A., Rudd, J.J., Salamov, A.,
719 Schmutz, J., Schouten, H.J., Shapiro, H., Stergiopoulos, I., Torriani, S.F., Tu,
720 H., de Vries, R.P., Waalwijk, C., Ware, S.B., Wiebenga, A., Zwiers, L.H., Oliver,
721 R.P., Grigoriev, I.V., and Kema, G.H. (2011) Finished genome of the fungal
722 wheat pathogen Mycosphaerella graminicola reveals dispensome structure,
723 chromosome plasticity, and stealth pathogenesis. *PLoS Genet* **7**: e1002070.
724 Grandaubert, J., Bhattacharyya, A., and Stukenbrock, E.H. (2015) RNA-seq-Based
725 Gene Annotation and Comparative Genomics of Four Fungal Grass Pathogens
726 in the Genus Zymoseptoria Identify Novel Orphan Genes and Species-Specific
727 Invasions of Transposable Elements. *G3 (Bethesda)* **5**: 1323-1333.
728 Habig, M., Quade, J., and Stukenbrock, E.H. (2017) Forward Genetics Approach
729 Reveals Host Genotype-Dependent Importance of Accessory Chromosomes in
730 the Fungal Wheat Pathogen Zymoseptoria tritici. *mBio* **8**.

731 Hiragami-Hamada, K., and Nakayama, J.I. (2019) Do the charges matter?-balancing
732 the charges of the chromodomain proteins on the nucleosome. *J Biochem* **165**:
733 455-458.
734 Huerta-Cepas, J., Forslund, K., Coelho, L.P., Szklarczyk, D., Jensen, L.J., von Mering,
735 C., and Bork, P. (2017) Fast Genome-Wide Functional Annotation through
736 Orthology Assignment by eggNOG-Mapper. *Mol. Biol. Evol.* **34**: 2115-2122.
737 Jih, G., Iglesias, N., Currie, M.A., Bhanu, N.V., Paulo, J.A., Gygi, S.P., Garcia, B.A.,
738 and Moazed, D. (2017) Unique roles for histone H3K9me states in RNAi and
739 heritable silencing of transcription. *Nature* **547**: 463-467.
740 Kellner, R., Bhattacharyya, A., Poppe, S., Hsu, T.Y., Brem, R.B., and Stukenbrock,
741 E.H. (2014) Expression profiling of the wheat pathogen Zymoseptoria tritici
742 reveals genomic patterns of transcription and host-specific regulatory
743 programs. *Genome Biol Evol* **6**: 1353-1365.
744 Keon, J., Antoniw, J., Carzaniga, R., Deller, S., Ward, J.L., Baker, J.M., Beale, M.H.,
745 Hammond-Kosack, K., and Rudd, J.J. (2007) Transcriptional adaptation of
746 Mycosphaerella graminicola to programmed cell death (PCD) of its susceptible
747 wheat host. *Mol Plant Microbe Interact* **20**: 178-193.
748 King, R., Urban, M., Lauder, R.P., Hawkins, N., Evans, M., Plummer, A., Halsey, K.,
749 Lovegrove, A., Hammond-Kosack, K., and Rudd, J.J. (2017) A conserved
750 fungal glycosyltransferase facilitates pathogenesis of plants by enabling hyphal
751 growth on solid surfaces. *PLoS Pathog* **13**: e1006672.
752 Kolde, R., (2019) pheatmap: Pretty Heatmaps. In., pp.
753 Krishnan, P., Meile, L., Plissonneau, C., Ma, X., Hartmann, F.E., Croll, D., McDonald,
754 B.A., and Sanchez-Vallet, A. (2018) Transposable element insertions shape

gene regulation and melanin production in a fungal pathogen of wheat. *BMC Biol* **16**: 78.

Kumar, A., and Kono, H. (2020) Heterochromatin protein 1 (HP1): interactions with itself and chromatin components. *Biophys Rev* **12**: 387-400.

Langmead, B., and Salzberg, S.L. (2012) Fast gapped-read alignment with Bowtie 2. *Nat. Methods* **9**: 357-359.

Laurent, B., Palaiokostas, C., Spataro, C., Moinard, M., Zehraoui, E., Houston, R.D., and Foulongne-Oriol, M. (2018) High-resolution mapping of the recombination landscape of the phytopathogen Fusarium graminearum suggests two-speed genome evolution. *Mol Plant Pathol* **19**: 341-354.

Lee, W.S., Rudd, J.J., Hammond-Kosack, K.E., and Kanyuka, K. (2014) Mycosphaerella graminicola LysM effector-mediated stealth pathogenesis subverts recognition through both CERK1 and CEBiP homologues in wheat. *Mol Plant Microbe Interact* **27**: 236-243.

Li, H., Handsaker, B., Wysoker, A., Fennell, T., Ruan, J., Homer, N., Marth, G., Abecasis, G., Durbin, R., and Genome Project Data Processing, S. (2009) The Sequence Alignment/Map format and SAMtools. *Bioinformatics* **25**: 2078-2079.

Liao, Y., Smyth, G.K., and Shi, W. (2014) featureCounts: an efficient general purpose program for assigning sequence reads to genomic features. *Bioinformatics* **30**: 923-930.

Love, M.I., Huber, W., and Anders, S. (2014) Moderated estimation of fold change and dispersion for RNA-seq data with DESeq2. *Genome Biol* **15**: 550.

Machida, S., Takizawa, Y., Ishimaru, M., Sugita, Y., Sekine, S., Nakayama, J.I., Wolf, M., and Kurumizaka, H. (2018) Structural Basis of Heterochromatin Formation by Human HP1. *Mol Cell* **69**: 385-397 e388.

780 Mamillapalli, A., Pathak, R.U., Garapati, H.S., and Mishra, R.K. (2013) Transposable
781 element 'roo' attaches to nuclear matrix of the Drosophila melanogaster. *J*
782 *Insect Sci* **13**: 111.
783 Marshall, R., Kombrink, A., Motteram, J., Loza-Reyes, E., Lucas, J., Hammond-
784 Kosack, K.E., Thomma, B.P., and Rudd, J.J. (2011) Analysis of two in planta
785 expressed LysM effector homologs from the fungus Mycosphaerella
786 graminicola reveals novel functional properties and varying contributions to
787 virulence on wheat. *Plant Physiol* **156**: 756-769.
788 Möller, M., Schotanus, K., Soyer, J.L., Haueisen, J., Happ, K., Stralucke, M., Happel,
789 P., Smith, K.M., Connolly, L.R., Freitag, M., and Stukenbrock, E.H. (2019)
790 Destabilization of chromosome structure by histone H3 lysine 27 methylation.
791 *PLoS Genet* **15**: e1008093.
792 Motteram, J., Kufner, I., Deller, S., Brunner, F., Hammond-Kosack, K.E., Nurnberger,
793 T., and Rudd, J.J. (2009) Molecular characterization and functional analysis of
794 MgNLP, the sole NPP1 domain-containing protein, from the fungal wheat leaf
795 pathogen Mycosphaerella graminicola. *Mol Plant Microbe Interact* **22**: 790-799.
796 Quinlan, A.R. (2014) BEDTools: The Swiss-Army Tool for Genome Feature Analysis.
797 *Curr Protoc Bioinformatics* **47**: 11 12 11-34.
798 Reyes-Dominguez, Y., Bok, J.W., Berger, H., Shwab, E.K., Basheer, A., Gallmetzer,
799 A., Scazzocchio, C., Keller, N., and Strauss, J. (2010) Heterochromatic marks
800 are associated with the repression of secondary metabolism clusters in
801 Aspergillus nidulans. *Mol Microbiol* **76**: 1376-1386.
802 Rudd, J.J. (2015) Previous bottlenecks and future solutions to dissecting the
803 Zymoseptoria tritici-wheat host-pathogen interaction. *Fungal Genet Biol* **79**: 24-
804 28.

805 Rudd, J.J., Kanyuka, K., Hassani-Pak, K., Derbyshire, M., Andongabo, A., Devonshire,
806 J., Lysenko, A., Saqi, M., Desai, N.M., Powers, S.J., Hooper, J., Ambroso, L.,
807 Bharti, A., Farmer, A., Hammond-Kosack, K.E., Dietrich, R.A., and Courbot, M.
808 (2015) Transcriptome and metabolite profiling of the infection cycle of
809 Zymoseptoria tritici on wheat reveals a biphasic interaction with plant immunity
810 involving differential pathogen chromosomal contributions and a variation on
811 the hemibiotrophic lifestyle definition. *Plant Physiol* **167**: 1158-1185.
812 Schotanus, K., Soyer, J.L., Connolly, L.R., Grandaubert, J., Happel, P., Smith, K.M.,
813 Freitag, M., and Stukenbrock, E.H. (2015) Histone modifications rather than the
814 novel regional centromeres of Zymoseptoria tritici distinguish core and
815 accessory chromosomes. *Epigenetics Chromatin* **8**: 41.
816 Sidhu, Y.S., Cairns, T.C., Chaudhari, Y.K., Usher, J., Talbot, N.J., Studholme, D.J.,
817 Csukai, M., and Haynes, K. (2015) Exploitation of sulfonylurea resistance
818 marker and non-homologous end joining mutants for functional analysis in
819 Zymoseptoria tritici. *Fungal Genet Biol* **79**: 102-109.
820 Smothers, J.F., and Henikoff, S. (2000) The HP1 chromo shadow domain binds a
821 consensus peptide pentamer. *Curr Biol* **10**: 27-30.
822 Song, Q., and Smith, A.D. (2011) Identifying dispersed epigenomic domains from
823 ChIP-Seq data. *Bioinformatics* **27**: 870-871.
824 Soyer, J.L., El Ghalid, M., Glaser, N., Ollivier, B., Linglin, J., Grandaubert, J.,
825 Balesdent, M.H., Connolly, L.R., Freitag, M., Rouxel, T., and Fudal, I. (2014)
826 Epigenetic control of effector gene expression in the plant pathogenic fungus
827 Leptosphaeria maculans. *PLoS Genet* **10**: e1004227.

828 Soyer, J.L., Grandaubert, J., Haueisen, J., Schotanus, K., and Stukenbrock, E.H.
829 (2019) In planta chromatin immunoprecipitation in Zymoseptoria tritici reveals
830 chromatin-based regulation of putative effector gene expression. *BioRxiv*.
831 Soyer, J.L., Rouxel, T., and Fudal, I. (2015) Chromatin-based control of effector gene
832 expression in plant-associated fungi. *Curr Opin Plant Biol* **26**: 51-56.
833 Steinberg, G. (2015) Cell biology of Zymoseptoria tritici: Pathogen cell organization
834 and wheat infection. *Fungal Genet Biol* **79**: 17-23.
835 Sun, L., Jing, Y., Liu, X., Li, Q., Xue, Z., Cheng, Z., Wang, D., He, H., and Qian, W.
836 (2020) Heat stress-induced transposon activation correlates with 3D chromatin
837 organization rearrangement in Arabidopsis. *Nat Commun* **11**: 1886.
838 Turck, F., Roudier, F., Farrona, S., Martin-Magniette, M.L., Guillaume, E., Buisine, N.,
839 Gagnot, S., Martienssen, R.A., Coupland, G., and Colot, V. (2007) Arabidopsis
840 TFL2/LHP1 specifically associates with genes marked by trimethylation of
841 histone H3 lysine 27. *PLoS Genet* **3**: e86.
842 Uhse, S., and Djamei, A. (2018) Effectors of plant-colonizing fungi and beyond. *PLoS*
843 *Pathog* **14**: e1006992.
844 Wickham, H. (2007) Reshaping Data with the reshape Package. *Journal of Statistical*
845 *Software* **21**: 1-20.
846 Wickham, H., Averick, M., Bryan, J., Chang, W., D'Agostino McGowan, L., François,
847 R., Grolemund, G., Hayes, A., Henry, L., Hester, J., Kuhn, M., Pedersen, T.,
848 Miller, E., Bache, S., Müller, K., Ooms, J., Robinson, D., Seidel, P., Spinu, V.,
849 Takahashi, K., Vaughan, D., Wilke, C., Woo, K., and Yutani, H. (2019) Welcome
850 to the tidyverse. *Journal of Open Source Software* **4**: 1686.

851 Yale, K., Tackett, A.J., Neuman, M., Bulley, E., Chait, B.T., and Wiley, E. (2016)
852 Phosphorylation-Dependent Targeting of Tetrahymena HP1 to Condensed
853 Chromatin. *mSphere* **1**.
854 Yap, K.L., and Zhou, M.M. (2011) Structure and mechanisms of lysine methylation
855 recognition by the chromodomain in gene transcription. *Biochemistry* **50**: 1966-
856 1980.
857 Zeng, W., Ball, A.R., Jr., and Yokomori, K. (2010) HP1: heterochromatin binding
858 proteins working the genome. *Epigenetics* **5**: 287-292.
859

FIGURE LEGENDS

Figure 1. Cbx1 is an HP1 homolog. Schematic representation of the domain architecture of Cbx1 showing the locations and theoretical pI values of the acidic N-terminal patch, chromodomain (CD), hinge, and chromoshadow domain (CSD) (top panel). Sequence alignment of the CD and CSD regions from the indicated fungal HP1 proteins was generated using CLUSTAL (middle and bottom panels). Full shading (black) represents conservation of an amino acid in at least 50% of the sequences, whilst grey shading denotes conservation of a residue of similar chemistry in at least 50% of the analysed sequences. Aromatic 'methyl-lysine cage' residues are coloured yellow and their positions are highlighted with asterisks.

Figure 2. Cbx1 binds H3K9me2/3. (A) GST-Cbx1 (1 μg) was incubated with the indicated biotinylated histone H3 peptide and streptavidin beads. Beads were recovered and co-precipitation of GST-Cbx1 was analyzed by western blotting using a GST specific antibody. A 10% input GST-Cbx1 was included as a reference. A representative of three biological repeats is shown. **(B)** Quantification of the GST-Cbx1 signal was relative to the 10% input. Data is the mean of three biological repeats and error bars are ±SEM. **(C)** Fluorescence microscopy of the *cbx1-GFP* strain. **(D)** Cbx1 is associated with H3K9me3 modified chromatin. Chromatin immunoprecipitation (ChIP)-qPCR was used to determine the enrichment of Cbx1-GFP at the indicated loci. The reference IPO323 (untagged) strain was included as a control. %IP was quantified relative to the input sample. Data is the mean of three biological repeats error bars are ±SEM.

884 **Figure 3. Deletion of *cbx1* and *kmt1* results in distinct phenotypes.** Cell
885 suspensions of the indicated strain were subjected to a five-fold serial dilution and
886 pinned onto the indicated agar plates and incubated at 18°C unless indicated
887 otherwise. Agar plates were made with YMS (Yeast extract, malt extract, sucrose) or
888 where indicated, PDA (potato dextrose agar). Concentrations of the stress-inducing
889 agents were, NaCl 1 M, sorbitol 1 M, calcofluor white (CFW) 50 µg/mL, congo red (CR)
890 150 µg/mL, H_2O_2 2 mM, UV dose 250 J/m^2, hydroxyurea (HU) 5 mM, Bleocin 250
891 ng/mL and Carboxin 2.5 ng/mL.

892

893 **Figure 4. *cbx1* deletion slows disease progression. (A)** Wheat leaves treated with
894 IPO323, the indicated Δ*cbx1* strains, and a mock infected leaf at 14 days post infection
895 (dpi). **(B)** Wheat leaves from (A) at 21 dpi. A large reduction in pycnidia was observed
896 in leaves treated with the Δ*cbx1* strains. The displayed leaves are representative of
897 three biological repeats. **(C)** Close up of leaves shown in (B).

898

899 **Figure 5. Global impact of Cbx1 and Kmt1 on the transcriptome (A)** Hierarchical
900 clustering analysis of the indicated RNA-seq samples. Clustering was performed
901 according to Pearson correlation with the complete linkage method and calculated on
902 log_2 normalised read counts. **(B)** An MA plot of mean normalised counts plotted
903 against log_2 fold change for all genes expressed in Δ*cbx1* and IPO323. Genes in red
904 indicate a statistically significant change in gene expression ($p<0.05$). Genes in grey
905 fall below the cut-off adjusted p value **(C)** An MA plot of Δ*kmt1* and IPO323. Details
906 as for (B). **(D)** Venn diagram comparing differentially expressed genes (>2-fold change
907 in expression, adjusted p value < 0.05) in Δ*cbx1* and Δ*kmt1*. The statistical significance

908 of the overlap was calculated using a Fisher's test based on hypergeometric
909 distribution. **(E)** As for (D) with up-regulated genes. **(F)** As for (D) with down-regulated
910 genes.

911

912 **Figure 6. Loss of Cbx1 does not result in a global increase of expression from**
913 **TEs and accessory chromosomes. (A)** Median sorted boxplots of Rlog normalised
914 read counts from genes on accessory chromosomes. n = number of genes/elements
915 analysed. * = $p < 0.05$, ns = not significant (ANOVA). **(B)** TE expression analysed
916 as described in (A) *** = $p < 0.001$ (ANOVA). **(C)** Hierarchical clustering analysis of
917 TE expression in the indicated RNA-seq samples. Clustering was performed according
918 to Pearson correlation with the complete linkage method and calculated on log_2
919 normalised read counts. **(D)** Genes associated (± 2Kb) with TE elements. Venn
920 diagram displaying proportions of TE-associated genes commonly and uniquely
921 differentially expressed in Δ*cbx1* and Δ*kmt1*. The statistical significance of the overlap
922 was calculated using a Fisher test based on hypergeometric distribution. **(E)** Heatmap
923 of TE-associated genes that are differentially expressed in both Δ*cbx1* and Δ*kmt1*.
924 The colour scale represents log_2 fold changes from -7 to 10. Genes linked to
925 secondary metabolism are indicated. Genes were clustered using euclidean distance
926 and complete linkage.

927

928 **Figure 7. The majority of H3K9me-associated genes are not differentially**
929 **expressed in Δ*cbx1* mutants. (A)** Venn diagram of genes differentially expressed
930 (DE) in Δ*cbx1* and genes associated with (> 1bp) H3K9me (B) Δ*cbx1* DE genes and
931 fully marked (100%) H3K9me genes. (C) Δ*kmt1* DE genes and H3K9me3 associated
932 genes. (D) Δ*kmt1* DE genes and H3K9me fully marked genes. The statistical

933 significance of the overlaps in each case was calculated using a Fisher's test based
934 on hypergeometric distribution.
935
936 **Figure 8. Cbx2, a fungal specific chromodomain protein that binds to H3K9me3**
937 ***in vitro*. (A)** Schematic representation of the domain architecture of Cbx2 showing the
938 location and theoretical pIs of the two chromodomains CD1 and CD2. **(B)** Fungal
939 species with close homologs of Cbx2. The organism, pathogenicity, family, number of
940 chromodomains (predicted by Prosite) and E value relative to Cbx2 are shown. **(C)**
941 GST-Cbx2 (αα 503-703) (1 μg) was incubated with the indicated biotinylated histone
942 H3 peptide and streptavidin beads. Beads were recovered and co-precipitation of
943 GST-Cbx2 was analyzed by western blotting using a GST specific antibody. A 10%
944 input GST-Cbx2 was included as a reference. A representative of three biological
945 repeats is shown. **(D)** Quantification of the GST-Cbx2 signal was relative to the 10%
946 input. Data is the mean of three biological repeats and error bars are ±SEM.
947
948 **Figure 9. Deletion of *cbx2* does not impair growth *in planta* (A)** Wheat leaves
949 treated with IPO323, Δ*cbx2* strains and a mock infection (M) at 14 dpi. **(B)** The same
950 wheat leaves at 21 dpi. The displayed leaves are representative of three biological
951 repeats. **(C)** Close up of the leaves shown in (B).
952
953 **Figure 10. Cbx1 and Cbx2 have redundant functions. (A)** The *in vitro* growth
954 defects of Δ*cbx1* Δ*cbx2* mutants are similar to Δ*kmt1*. Cell suspensions of the
955 indicated strain were subjected to a five-fold serial dilution and pinned onto the
956 indicated agar plates. Abbreviations and concentrations are as described for Figure 3.
957 **(B)** RNA was extracted from the indicated strains. Mycgr3103556 mRNA levels were

958 determined by RT-qPCR, normalised to actin (Mycgr3G105948) mRNA and scaled
959 relative to the wild type (IPO323) level. Data are the mean of ≥ 3 independent
960 biological repeats and error bars represent ±SEM. **(C)** Mycgr3G44980 mRNA levels
961 were determined as described in (B).
962
963 **Figure S1. Deletion of *kmt1* results in loss of H3K9me3 and virulence**
964 **Figure S2. Principal component analysis (PCA) analysis of RNA-seq data**
965 **Figure S3. Differentially expressed (DE) genes in Δ*kmt1* overlap with DE genes**
966 **in the Zt09-Δ*kmt1* strain (Moller *et al.*, 2019).**
967 **Figure S4. Comparison of Cbx2 chromodomains with HP1 chromodomains.**
968 **Figure S5. Sequence alignments of Cbx2 homologs**
969 **Figure S6. *In vitro* growth phenotypes of Δ*cbx2* mutants**
970
971 **Table S1. Genes differentially expressed in Δ*kmt1***
972 **Table S2. Genes differentially expressed in Δ*cbx1***
973 **Table S3. Genes differentially expressed in Δ*cbx1* but not Δ*kmt1***
974 **Table S4. Genes differentially expressed in Δ*kmt1* but not Δ*cbx1***
975 **Table S5. Oligonucleotide primers used for qPCR in this study.**

Cbx1 (239 αα)

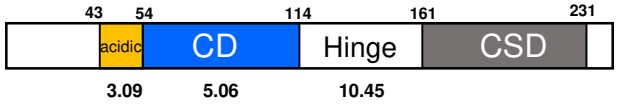

CD

CSD

Figure 1

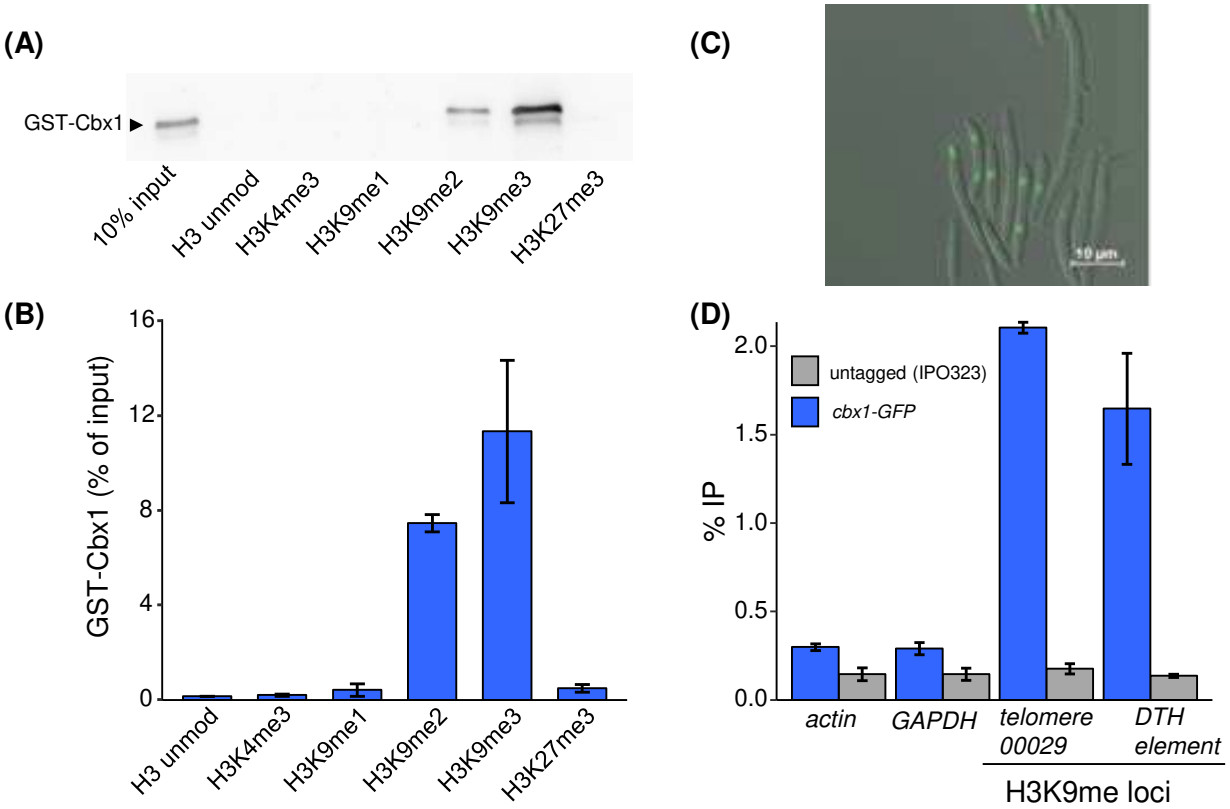
(A)
GST-Cbx1
10% input
H3 unmod
H3K4me3
H3K9me1
H3K9me2
H3K9me3
H3K27me3
(C)
(B)
GST-Cbx1 (% of input)
16
12
8
4
0
H3 unmod
H3K4me3
H3K9me1
H3K9me2
H3K9me3
H3K27me3
(D)
% IP
2.0
1.5
1.0
0.5
0.0
untagged (IPO323)
cbx1-GFP
actin
GAPDH
telomere 00029
DTH element
H3K9me loci

Figure 2

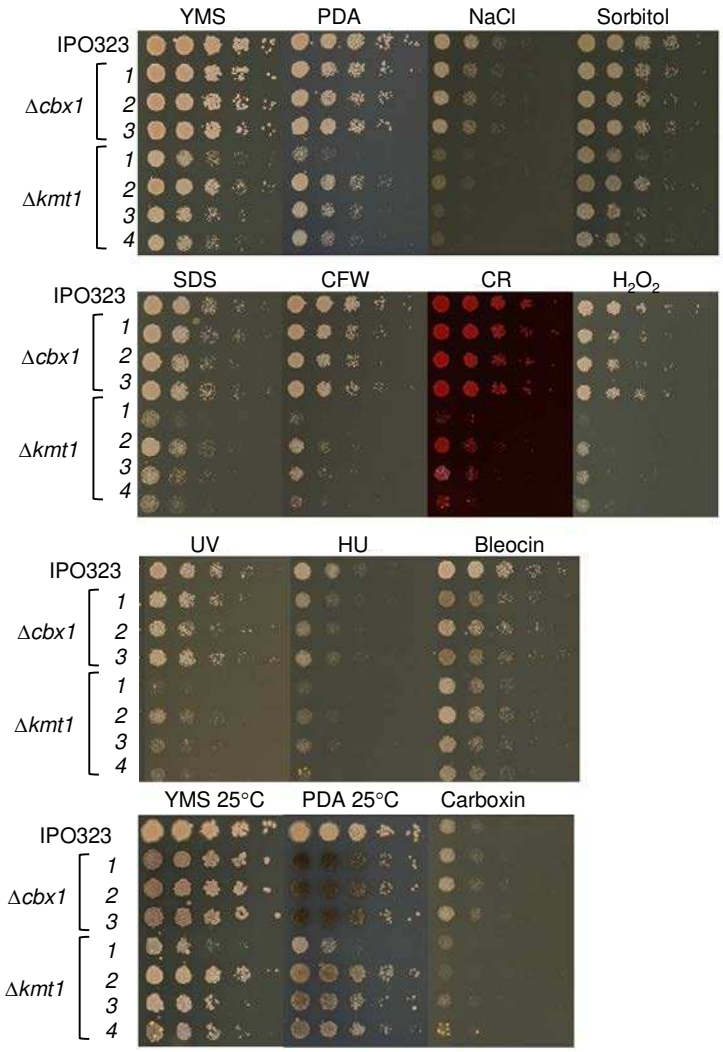
YMS
PDA
NaCl
Sorbitol
IPO323
Δcbx1
1
2
3
Δkmt1
1
2
3
4
SDS
CFW
CR
H2O2
UV
HU
Bleocin
YMS 25°C
PDA 25°C
Carboxin

Figure 3

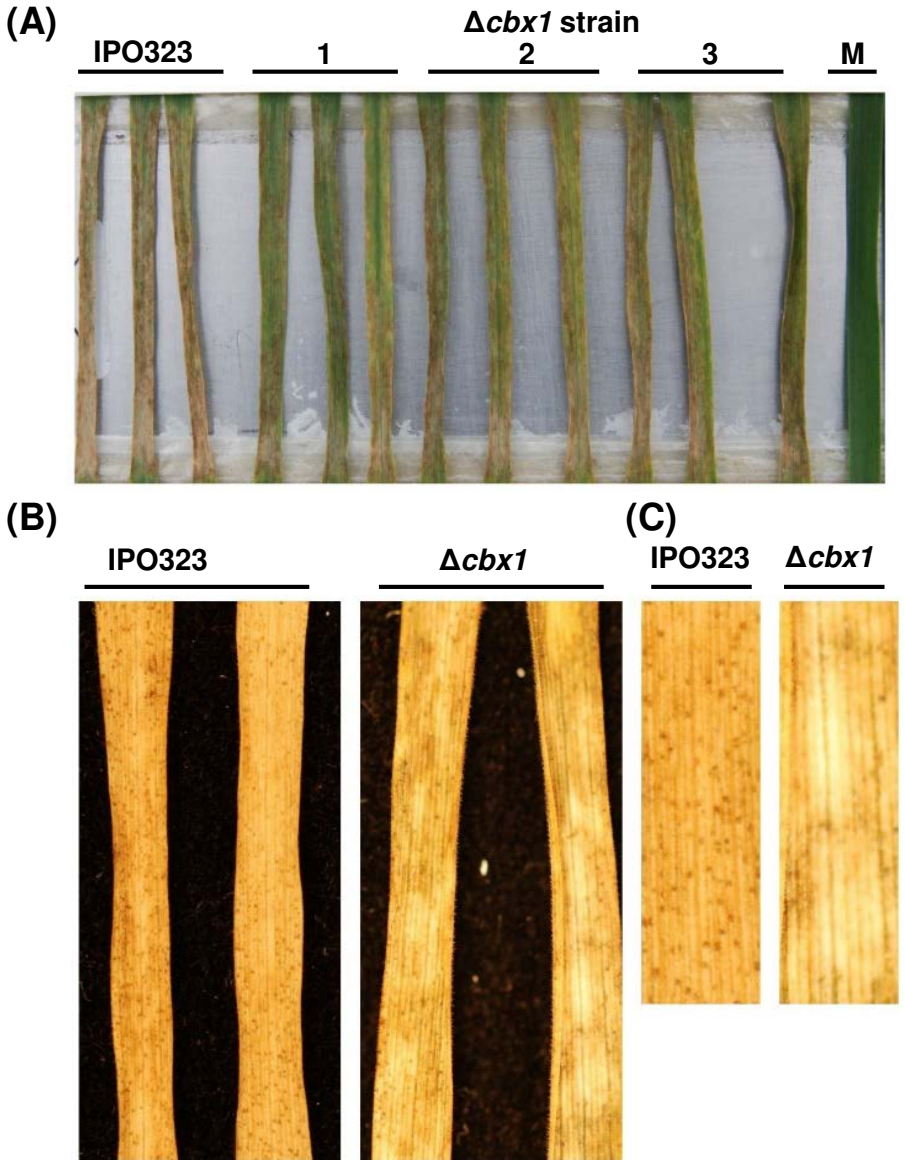

Figure 4

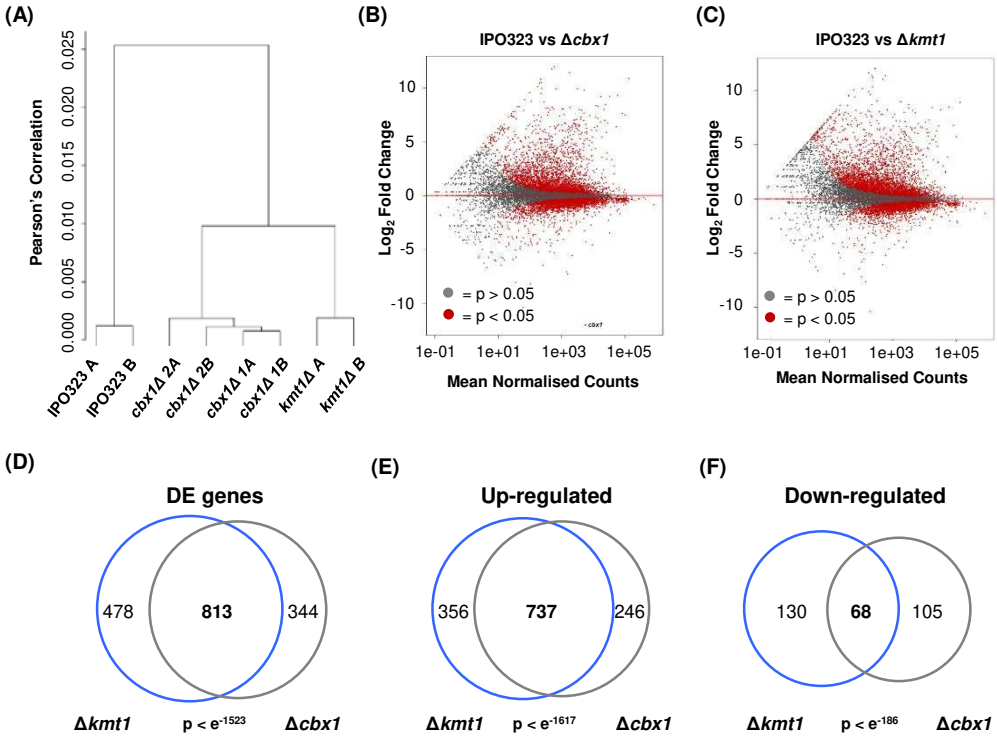
(A)
Pearson's Correlation
0.025
0.020
0.015
0.010
0.005
0.000
IPO323 A
IPO323 B
cbx1Δ 2A
cbx1Δ 2B
cbx1Δ 1A
cbx1Δ 1B
kmt1Δ A
kmt1Δ B
(B)
IPO323 vs Δcbx1
Log2 Fold Change
10
5
0
-5
-10
= p > 0.05
= p < 0.05
1e-01
1e+01
1e+03
1e+05
Mean Normalised Counts
(C)
IPO323 vs Δkmt1
Log2 Fold Change
10
5
0
-5
-10
= p > 0.05
= p < 0.05
1e-01
1e+01
1e+03
1e+05
Mean Normalised Counts

(D)
DE genes
478
813
344
Δkmt1
p < e-1523
Δcbx1
(E)
Up-regulated
356
737
246
Δkmt1
p < e-1617
Δcbx1
(F)
Down-regulated
130
68
105
Δkmt1
p < e-186
Δcbx1

Figure 5

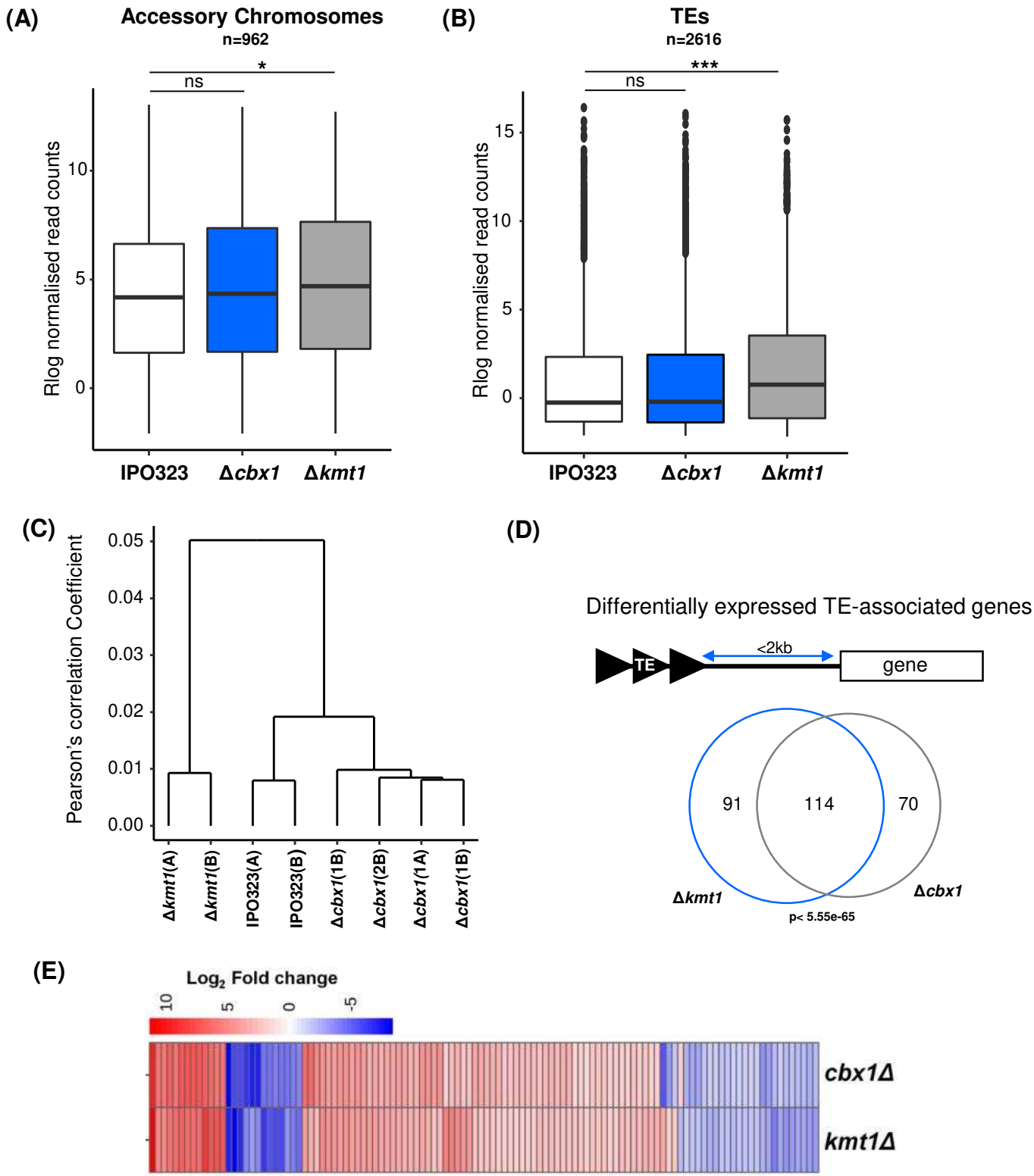
(A)
Accessory Chromosomes
n=962
ns
*
Rlog normalised read counts
IPO323
Δcbx1
Δkmt1
(B)
TEs
n=2616
ns
***
Rlog normalised read counts
IPO323
Δcbx1
Δkmt1
(C)
Pearson's correlation Coefficient
Δkmt1(A)
Δkmt1(B)
IPO323(A)
IPO323(B)
Δcbx1(1B)
Δcbx1(2B)
Δcbx1(1A)
Δcbx1(1B)
(D)
Differentially expressed TE-associated genes
TE
<2kb
gene
91
114
70
Δkmt1
Δcbx1
p< 5.55e-65
(E)
Log2 Fold change
cbx1Δ
kmt1Δ

Figure 6

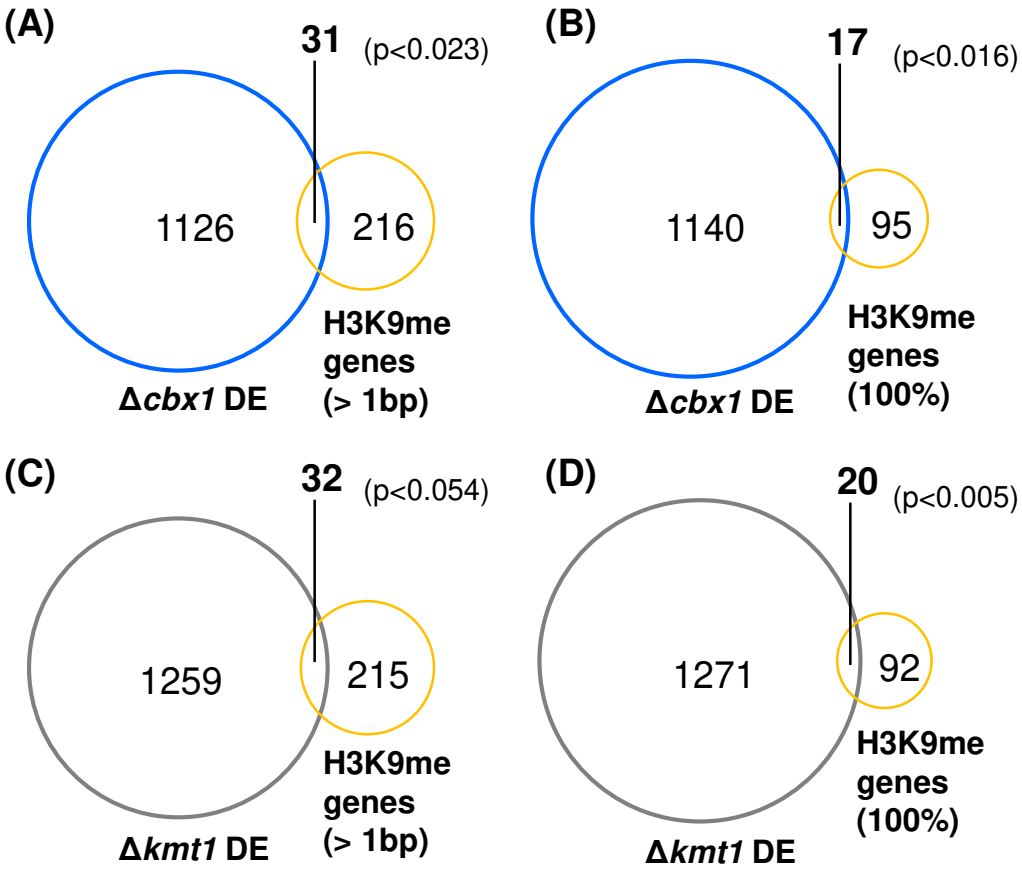
(A)
31
(p<0.023)
1126
216
H3K9me genes (> 1bp)
Δcbx1 DE
(B)
17
(p<0.016)
1140
95
H3K9me genes (100%)
Δcbx1 DE
(C)
32
(p<0.054)
1259
215
H3K9me genes (> 1bp)
Δkmt1 DE
(D)
20
(p<0.005)
1271
92
H3K9me genes (100%)
Δkmt1 DE

Figure 7

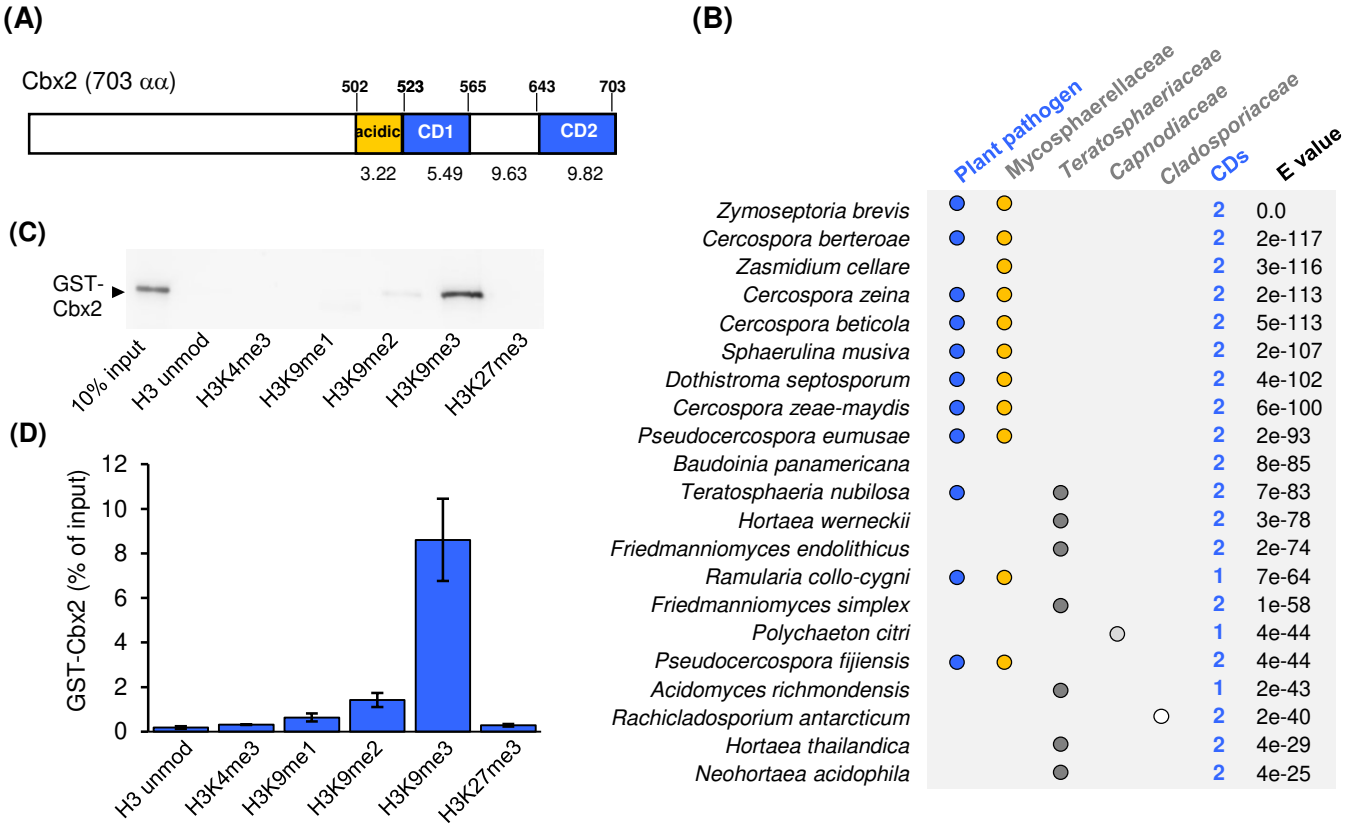
(A)
Cbx2 (703 αα)
502
523
565
643
703
acidic
CD1
CD2
3.22
5.49
9.63
9.82
(B)
Plant pathogen
Mycosphaerellaceae
Teratosphaeriaceae
Capnodiaceae
Cladosporiaceae
CDs
E value
Zymoseptoria brevis 2 0.0
Cercospora berteroae 2 2e-117
Zasmidium cellare 2 3e-116
Cercospora zeina 2 2e-113
Cercospora beticola 2 5e-113
Sphaerulina musiva 2 2e-107
Dothistroma septosporum 2 4e-102
Cercospora zeae-maydis 2 6e-100
Pseudocercospora eumusae 2 2e-93
Baudoinia panamericana 2 8e-85
Teratosphaeria nubilosa 2 7e-83
Hortaea werneckii 2 3e-78
Friedmanniomyces endolithicus 2 2e-74
Ramularia collo-cygni 1 7e-64
Friedmanniomyces simplex 2 1e-58
Polychaeton citri 1 4e-44
Pseudocercospora fijiensis 2 4e-44
Acidomyces richmondensis 1 2e-43
Rachicladosporium antarcticum 2 2e-40
Hortaea thailandica 2 4e-29
Neohortaea acidophila 2 4e-25
(C)
GST-Cbx2
10% input
H3 unmod
H3K4me3
H3K9me1
H3K9me2
H3K9me3
H3K27me3
(D)
GST-Cbx2 (% of input)
0
2
4
6
8
10
12
H3 unmod
H3K4me3
H3K9me1
H3K9me2
H3K9me3
H3K27me3

Figure 8

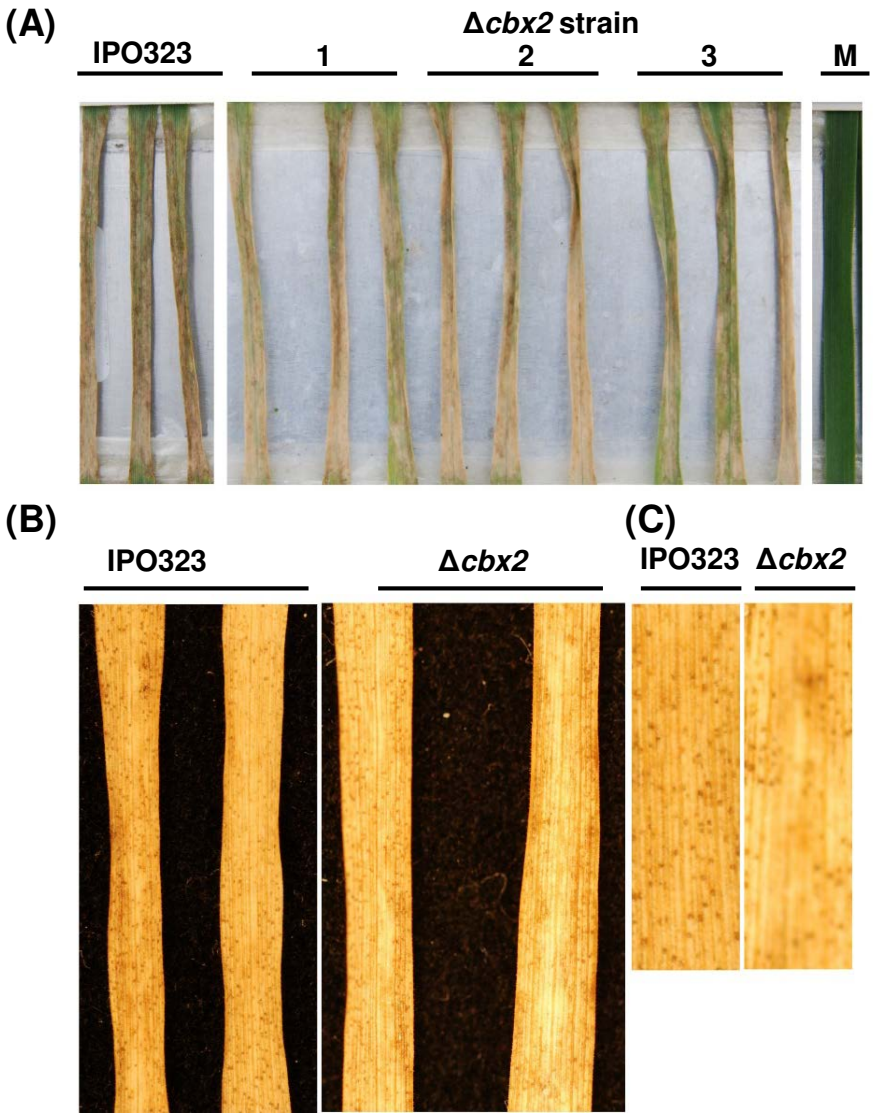

Figure 9

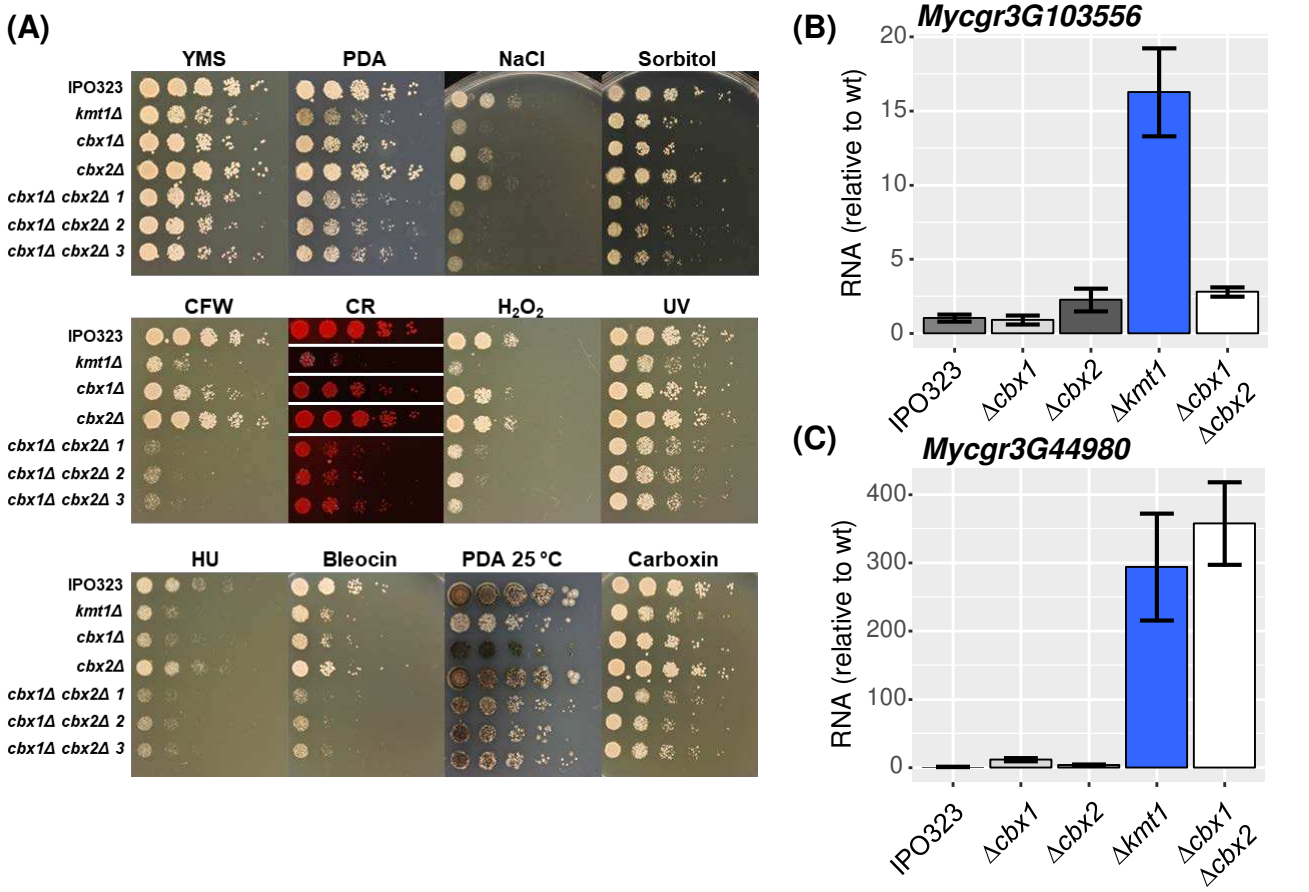
(A)
YMS
PDA
NaCl
Sorbitol
IPO323
kmt1Δ
cbx1Δ
cbx2Δ
cbx1Δ cbx2Δ 1
cbx1Δ cbx2Δ 2
cbx1Δ cbx2Δ 3
CFW
CR
H2O2
UV
HU
Bleocin
PDA 25 °C
Carboxin
(B)
Mycgr3G103556
RNA (relative to wt)
20
15
10
5
0
IPO323
Δcbx1
Δcbx2
Δkmt1
Δcbx1 Δcbx2
(C)
Mycgr3G44980
400
300
200
100

Figure 10